Check for updates

Received: 20 July 2023 | Revised: 24 October 2023 | Accepted: 1 January 2024

DOI: 10.1111/apha.14086

ACTA PHYSIOLOGICA

RESEARCH PAPER

IP3RPEP6, a novel peptide inhibitor of IP_3 receptor channels that does not affect connexin-43 hemichannels

Siyu Tao[1] | **Paco Hulpiau**[2] | **Larry E. Wagner II**[3] | **Katja Witschas**[1] | **David I. Yule**[3] | **Geert Bultynck**[4] | **Luc Leybaert**[1]

[1]Department of Basic and Applied Medical Sciences—Physiology Group, Ghent University, Ghent, Belgium

[2]Department of Bio-Medical Sciences, HOWEST University of Applied Sciences (Hogeschool West-Vlaanderen), Bruges, Belgium

[3]Department of Pharmacology and Physiology, School of Medicine and Dentistry, University of Rochester Medical Center, Rochester, New York, USA

[4]Laboratory of Molecular and Cellular Signaling, Department of Molecular Cell Biology, KU Leuven, Leuven, Belgium

Correspondence
Luc Leybaert, Department of Basic and Applied Medical Sciences—Physiology Group, Ghent University, Ghent 9000, Belgium.
Email: luc.leybaert@ugent.be

Funding information
China Scholarship Council, Grant/Award Number: 201906170050; Onderzoeksraad, KU Leuven, Grant/Award Number: C14/19/099 and AKUL/19/34; Fonds Wetenschappelijk Onderzoek, Grant/Award Number: G052718N, G040720N, G063023N, G090118N, G0E7520N, G081821N, G094522N, W0.019.17N and W0.014.22N

Abstract

Aim: Inositol 1,4,5-trisphosphate receptors (IP_3Rs) are intracellular Ca^{2+}-release channels with crucial roles in cell function. Current IP_3R inhibitors suffer from off-target effects and poor selectivity towards the three distinct IP_3R subtypes. We developed a novel peptide inhibitor of IP_3Rs and determined its effect on connexin-43 (Cx43) hemichannels, which are co-activated by IP_3R stimulation.

Methods: IP3RPEP6 was developed by in silico molecular docking studies and characterized by on-nucleus patch-clamp experiments of IP_3R2 channels and carbachol-induced IP_3-mediated Ca^{2+} responses in IP_3R1, 2 or 3 expressing cells, triple IP_3R KO cells and astrocytes. Cx43 hemichannels were studied by patch-clamp and ATP-release approaches, and by inhibition with Gap19 peptide. IP3RPEP6 interactions with IP_3Rs were verified by co-immunoprecipitation and affinity pull-down assays.

Results: IP3RPEP6 concentration-dependently reduced the open probability of IP_3R2 channels and competitively inhibited IP_3Rs in an IC_{50} order of IP_3R2 (~3.9 μM) < IP_3R3 (~4.3 μM) < IP_3R1 (~9.0 μM), without affecting Cx43 hemichannels or ryanodine receptors. IP3RPEP6 co-immunoprecipitated with IP_3R2 but not with IP_3R1; interaction with IP_3R3 varied between cell types. The IC_{50} of IP3RPEP6 inhibition of carbachol-induced Ca^{2+} responses decreased with increasing cellular Cx43 expression. Moreover, Gap19-inhibition of Cx43 hemichannels significantly reduced the amplitude of the IP_3-Ca^{2+} responses and strongly increased the EC_{50} of these responses. Finally, we identified palmitoyl-8G-IP3RPEP6 as a membrane-permeable IP3RPEP6 version allowing extracellular application of the IP_3R-inhibiting peptide.

Conclusion: IP3RPEP6 inhibits $IP_3R2/R3$ at concentrations that have limited effects on IP_3R1. IP_3R activation triggers hemichannel opening, which strongly affects the amplitude and concentration-dependence of IP_3-triggered Ca^{2+} responses.

Katja Witschas, Geert Bultynck and Luc Leybaert shared senior authorship.

This is an open access article under the terms of the Creative Commons Attribution License, which permits use, distribution and reproduction in any medium, provided the original work is properly cited.
© 2024 The Authors. *Acta Physiologica* published by John Wiley & Sons Ltd on behalf of Scandinavian Physiological Society.

KEYWORDS
astrocytes, Ca^{2+} signaling, connexin-43, hemichannel, inositol 1,4,5-trisphosphate, IP_3, peptide inhibitor

1 | INTRODUCTION

Inositol 1,4,5-trisphosphate receptors (IP_3Rs) are tetrameric Ca^{2+} permeable channels primarily located at the membrane of the endoplasmic reticulum (ER).[1–3] Numerous physiological processes are controlled by Ca^{2+}-mediated signaling through IP_3Rs.[4,5] Mammalian cells express three distinct IP_3R subtypes, namely IP_3R1, IP_3R2 and IP_3R3, which possess ~70% homology. IP_3Rs operate at the heart of molecular signaling networks and affect metabolic cellular homeostasis.[6–8] However, current understanding of IP_3R-related diseases remains limited and is hampered by a lack of selective pharmacological tools targeting these receptors.

Each IP_3R monomer contains a suppressor region, an IP_3 binding core, a regulatory region, a transmembrane region and a C-terminal region,[9–11] organized in a "mushroom-like" structure. There are currently no IP_3R antagonists without side effects.[12,13] Heparin,[14] 2-aminoethoxydiphenyl borate (2-APB),[15] caffeine,[16] and Xestospongins[17] are widely used to inhibit IP_3-evoked Ca^{2+} release, but each of those compounds has shortcomings in terms of selectivity and side effects.[18,19] Starting the search for novel candidate inhibitors based on endogenous protein sequences seems promising, as exemplified by work showing Bcl-2 BH4 domain interaction with the IP_3R1 ligand-binding site thereby inhibiting channel function.[20] Here, we started from a regulatory mechanism in IP_3R3 whereby a loop extending from a so-called "ARM2" structure between the α_{ARM2}-1 and α_{ARM2}-2 domain binds to the IP_3-binding site and competitively inhibits IP_3 binding,[21] providing crucial insights into the mechanistic function of IP_3Rs and subtype-specific regulation of these important Ca^{2+}-release channels.

The IP_3-Ca^{2+} signaling axis has many cross-points with connexins, for example, intercellular Ca^{2+} waves are mediated by IP_3 diffusion through gap junctions (reviewed in Ref. [22]). IP_3-Ca^{2+} signaling furthermore underlies oscillations of the intracellular Ca^{2+} concentration ($[Ca^{2+}]_i$) in response to a myriad of trigger conditions (reviewed in Ref. [3]), in which the bell-shaped $[Ca^{2+}]_i$-dependence of IP_3R channel opening is a crucial factor.[23–25] Cx43 hemichannels also have a bell-shaped $[Ca^{2+}]_i$-dependence for their opening,[26] allowing them to contribute to Ca^{2+} oscillations by Ca^{2+} entry.[26–30] Stimulation of IP_3R signaling furthermore enhances gap junction coupling[12] but also affects hemichannels, that is, the precursor channels of gap junctions, which are more strongly activated to open in response to IP_3-triggered $[Ca^{2+}]_i$ elevation than by Ca^{2+} entry.[31] Open hemichannels permeate substances below ~1.5 kDa, allowing Ca^{2+} and Na^{+}[32–36] entry but also the loss of, for example, intracellular ATP[37,38] and IP_3.[39] Because IP_3-Ca^{2+} signaling strongly activates hemichannel opening, a second aim of the present paper was to determine to what extent Cx43 hemichannel opening contributed to IP_3-triggered Ca^{2+} responses.

Here, we investigated IP3RPEP6 derived from the ARM2 structure of IP_3R2 that interacts with the IP_3-binding site and competitively inhibits IP_3 binding and subsequent Ca^{2+}-channel activation. Our results demonstrate that IP3RPEP6 inhibits activation of IP_3R2 and IP_3R3 with more limited effects on IP_3R1. Activation of IP_3-Ca^{2+} signaling also triggers Cx43 hemichannel

FIGURE 1 IP3RPEP6 decreases IP_3R2 single-channel open probability in a concentration-dependent manner. (A) Domain topology within the human IP_3R3 monomer, illustrating the ligand-binding domain and the domain containing the self-binding peptide (SBP). Numbers reflect amino acid positions. TMDs, transmembrane domains. (B) Sequence alignment of part of the regulatory ARM2 domain of human type-1, -2 and -3 IP_3Rs containing the SBP sequence. The α-helical cylinders left and right represent the arms holding the interposed SBP stretch, which is brought in the vicinity of the IP_3 binding site.[21] (C) Peptides used in the present study. (D) Representative IP_3R2 single-channel recordings from DT40-TKO cells stably expressing IP_3R2. Channel activity was evoked by 1 μM IP_3 at 200 nM Ca^{2+} and 5 mM ATP in the presence of phosphate-buffered saline (PBS) or in the presence of IP3RPEP6 or IP3RPEP6-E2A at the concentration indicated; C, closed state; O, open state. (E) Pooled data plotted as the $P_o \pm$SEM for the IP_3R2 current recordings (PBS, $N=5$; 1 μM IP3RPEP6, $N=6$; 10 μM IP3RPEP6, $N=5$; 50 μM IP3RPEP6, $N=3$; 50 μM IP3RPEP6-E2A, $N=6$). Statistically significant differences were determined using a one-way ANOVA, with Dunnett's post-test ($^{\dagger}p<0.01$, $^{****}p<0.0001$ versus PBS control). IP3RPEP6-E2A lacking the two Glu residues had no significant effects. (F) Analysis of IP_3R2 burst kinetics. Mean burst length constants (solid symbols) and interburst interval time constants (open symbols) are plotted for all conditions. The data indicate that IP3RPEP6 inhibits IP_3R2 activity by increasing the interburst intervals without altering burst length; IP3RPEP6-E2A did not affect burst/interburst properties.

17481716, 0, Downloaded from https://onlinelibrary.wiley.com/doi/10.1111/apha.14086 by Ku Leuven, Wiley Online Library on [02/02/2024]. See the Terms and Conditions (https://onlinelibrary.wiley.com/terms-and-conditions) on Wiley Online Library for rules of use; OA articles are governed by the applicable Creative Commons License

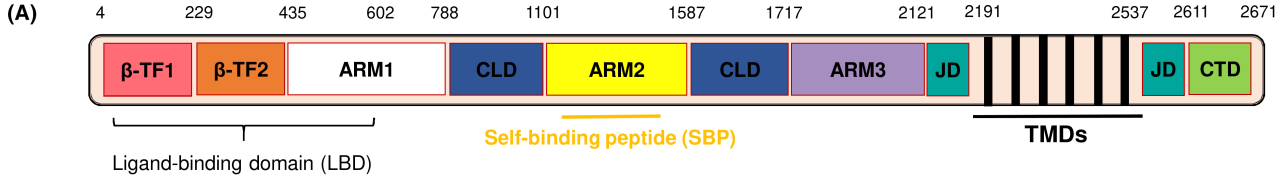

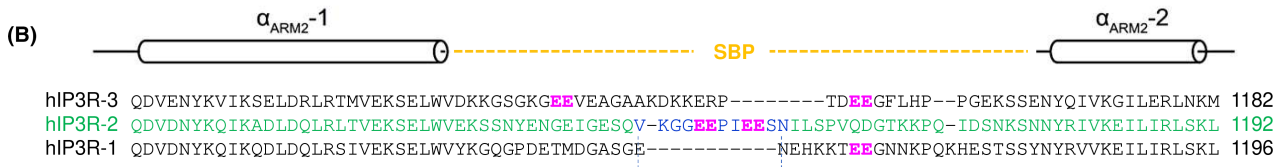

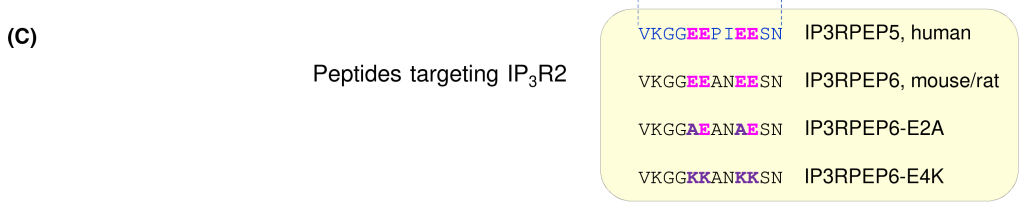

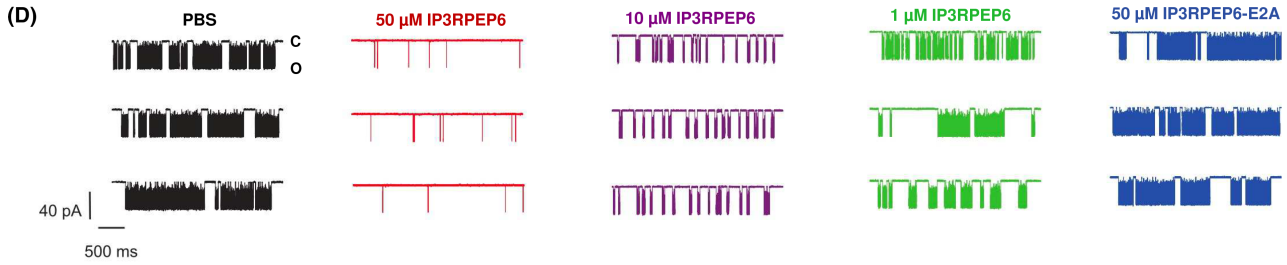

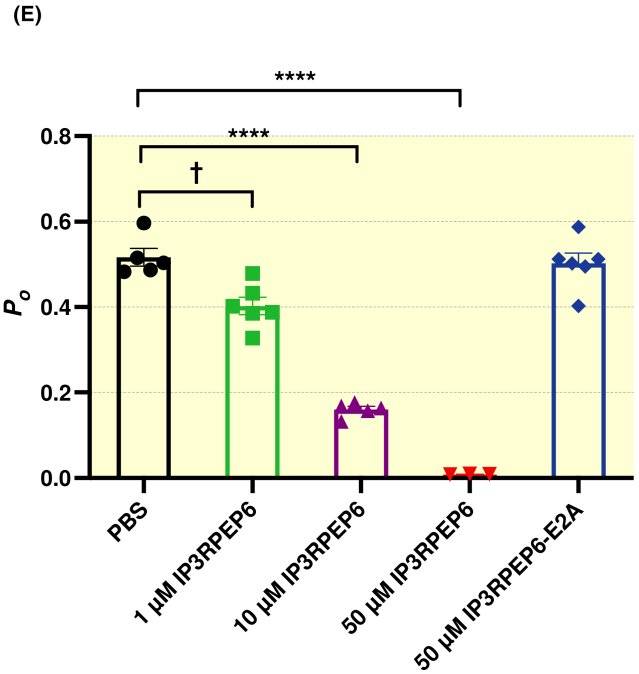

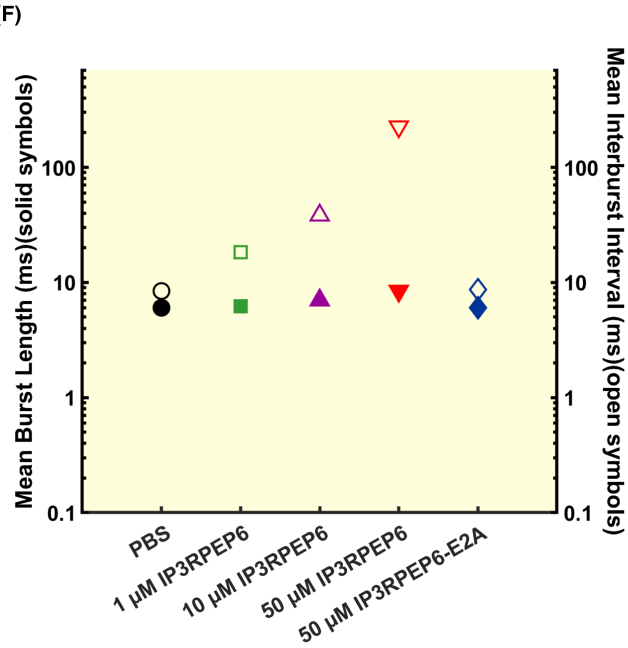

opening that acts to enhance and reshape the $[Ca^{2+}]_i$ responses. IP3RPEP6 had no effect on Cx43 hemichannel nor RyR activation and therefore reliably reports effects at the level of IP_3Rs. Taken together, our work brings up IP3RPEP6 as a new IP_3R inhibiting peptide primarily targeting $IP_3R2/3$ and not affecting co-players like ryanodine receptors or Cx43 hemichannels.

2 | RESULTS

2.1 | In silico approaches leading to IP3RPEP6 as a potential IP_3R2 antagonist

A cryo-EM structure of human IP_3R3 revealed the presence of a self-binding peptide (SBP) competing with

17481716, 0, Downloaded from https://onlinelibrary.wiley.com/doi/10.1111/apha.14086 by Ku Leuven, Wiley Online Library on [02/02/2024]. See the Terms and Conditions (https://onlinelibrary.wiley.com/terms-and-conditions) on Wiley Online Library for rules of use; OA articles are governed by the applicable Creative Commons License

IP_3 for binding to the IP_3 receptor site.[21] This SBP sequence is located at the end of two α-helical arms projecting from the N-terminal domain known as "ARM2" of IP_3R3 (Figure 1A); it occupies the IP_3-binding site and reduces the sensitivity of IP_3R3 to IP_3.[21] Sequence alignment showed that the SBP sequence for IP_3R2 contained an additional stretch of amino acids absent in IP_3R1 and partly lacking in IP_3R3 (Figure 1B). Within the putative SBP sequence of IP_3R2, we identified a cluster of closely apposed glutamate (Glu, E) residues and delineated several candidate peptides that were tested with PEP-SiteFinder[40,41] for their interaction with a homology model of the human IP_3R2 protein constructed with Modeller software.[42] Hereby, two peptides emerged with high interaction scores with the IP_3-binding site of IP_3R2: IP3RPEP5 (human) and IP3RPEP6 (mouse/rat version) (Figure 1C). Both peptides contained 4 Glu residues on a total of 12 amino acids, organized as two doublets separated by two other residues (double EE motif); IP3RPEP6 was chosen for further characterization.

2.2 | IP3RPEP6 inhibits IP_3R2 single-channel opening activity

We tested the effect of IP3RPEP6 on IP_3R2 single-channel activity using the on-nucleus patch-clamp approach on nuclei isolated from DT40-TKO cells stably expressing mouse IP_3R2.[43,44] Channel opening was triggered by 1 μM IP_3 in the presence of 200 nM $[Ca^{2+}]_i$ and 5 mM ATP to attain maximal achievable open probability (P_o), and we tested concentration-dependent IP3RPEP6 effects on single IP_3R2 channel opening activity (Figure 1D). IP3RPEP6 significantly decreased P_o and reciprocally extended interburst intervals in a concentration-dependent manner without affecting the mean burst length (Figure 1E,F). IP3RPEP6 inhibited IP_3R2 single channel activity by stabilizing a long-lived closed state with no influence on the mean open and closed times within bursts (Figure S1). In contrast, a control peptide in which the N-terminal Glu of each Glu doublet in IP3RPEP6 were changed into Ala (further called IP3RPEP6-E2A; Figure 1C) did not inhibit IP_3R2 single-channel activity (Figure 1D–F).

2.3 | IP3RPEP6 inhibits carbachol-triggered $[Ca^{2+}]_i$ elevation most potently for IP_3R2 and IP_3R3

To test IP3RPEP6 for its potential to inhibit IP_3-induced Ca^{2+} signals, we first characterized Ca^{2+} responses of HEK-293 cells selectively expressing human IP_3R1, IP_3R2 or IP_3R3.[45,46] We determined concentration-dependent responses of the three cell types to carbachol concentrations ranging from 0.1 to 1000 μM by $[Ca^{2+}]_i$ recording in Fluo-4 loaded cells (Figure 2A–F). The $[Ca^{2+}]_i$ response amplitude decreased in the order $IP_3R2 > IP_3R3 > IP_3R1$ (Figure 2A–C). The EC_{50} for $[Ca^{2+}]_i$ elevation was below 1 μM for IP_3R2, ~10 μM for IP_3R3 and almost 50 μM for IP_3R1 (Figure 2D–F). Ca^{2+} responses were absent in HEK-TKO cells in which all three IP_3 receptors were knocked out (Figure S2A). Subsequently, we explored a range of IP3RPEP6 concentrations to inhibit carbachol-induced Ca^{2+} responses. Due to the net negative charge, the peptide is poorly membrane-permeable, so we applied in situ electroporation for loading the peptide into the cells[47–49] and added dextran-tetramethyl-rhodamine reporter dye (100 μM) to identify peptide-loaded cells during $[Ca^{2+}]_i$ imaging. Intracellular loading efficiency of IP3RPEP6 was ~16% of the concentration applied outside on the electroporation electrode (Figure S3). Figure 2G–I illustrates concentration-dependent IP3RPEP6 inhibition of carbachol-induced Ca^{2+} responses in the different HEK-IP_3R cells, using submaximal carbachol stimulation. The strongest effects were observed for IP_3R2 and IP_3R3, with less complete inhibition for IP_3R1 delivering only ~⅔ inhibition at high (~100 μM) concentration (Figure 2G). The IC_{50} increased in the order IP_3R2 (~3.9 μM) < IP_3R3 (~4.3 μM) < IP_3R1 (~9.0 μM). Negative Hill slopes were ~3 for IP_3R2 and R3 and lower for IP_3R1 (~1.6). The control peptide IP3RPEP6-E2A did not inhibit IP_3R2-mediated $[Ca^{2+}]_i$ responses across a broad range of IP3RPEP6 concentrations (Figures S2B and S4 illustrates IP_3-evoked Ca^{2+} release in permeabilized HEK-IP_3R2 cells using MagFluo4 ER Ca^{2+} recording). Likewise, a peptide in which all 4 Glu residues were replaced by Lys (IP3RPEP6-E4K; Figure 1C) neither inhibited the responses (green datapoint in Figure S2B). The higher IC_{50} and smooth Hill slope for IP3RPEP6 inhibition of IP_3R1 is likely the result of the absence of the double EE motif in the SBP sequence of this receptor (see Figure 1B); in contrast, IP_3R3 contains the double EE motif but with a larger spatial separation compared to IP_3R2 (Figure 1B). We further tested IP3RPEP5 (human sequence containing a 'PI' instead of 'AN', see Figure 1B), which inhibited HEK-IP_3R2 responses with an IC_{50} of ~11 μM and a negative Hill slope of ~1, i.e. less favorable properties compared to IP3RPEP6.

2.4 | IP3RPEP6 competitively inhibits IP_3R2

To characterize competition between IP3RPEP6 and IP_3, we stimulated HEK-IP_3R2 cells with carbachol

17481716, 0, Downloaded from https://onlinelibrary.wiley.com/doi/10.1111/apha.14086 by Ku Leuven, Wiley Online Library on [02/02/2024]. See the Terms and Conditions (https://onlinelibrary.wiley.com/terms-and-conditions) on Wiley Online Library for rules of use; OA articles are governed by the applicable Creative Commons License

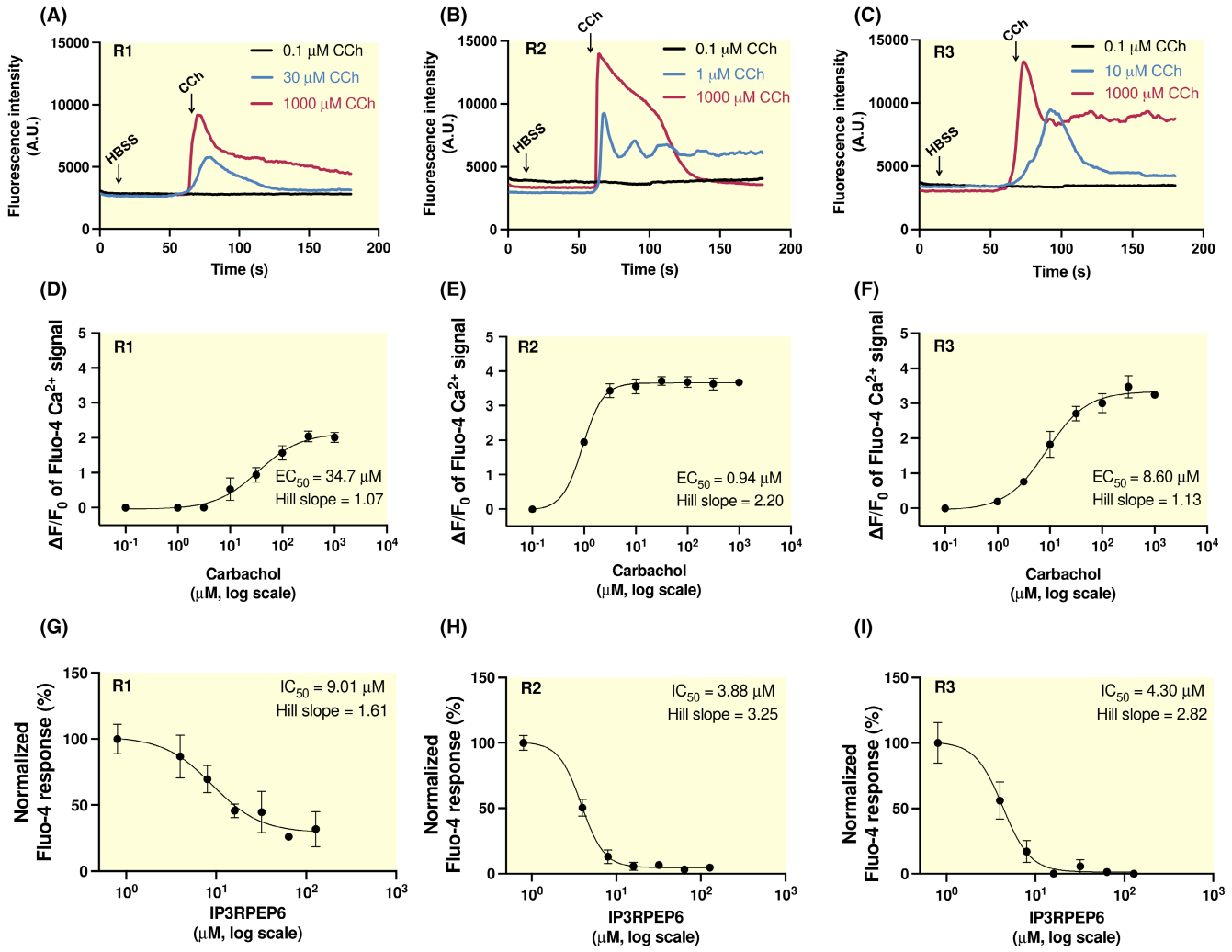

FIGURE 2 Concentration-dependent IP3RPEP6 inhibition of carbachol-induced Ca^{2+} elevation in HEK-IP_3R1, R2 and R3. Panels A–C show representative Ca^{2+} traces while D–F summarize concentration-response curves for carbachol-induced Ca^{2+} changes in HEK-IP_3R1, R2 and R3 cells. CCh indicates carbachol addition and HBSS refers to perfusion with vehicle solution. Data are expressed as mean ± SEM (IP_3R1, $N = 3$; IP_3R2, $N = 5$; IP_3R3, $N = 3$; $n = 5$ for each). (G–I) IP3RPEP6 inhibition was close to complete for IP_3R2, complete for IP_3R3 and less so for IP_3R1 where the curve leveled off at ~1/3 of the control response. IC_{50} was lowest for IP_3R2, slightly higher for IP_3R3 and much higher for IP_3R1. Negative Hill slopes were ~3 for IP_3R2/3 and much lower for IP_3R1. Data are expressed as the mean ± SEM ($N = 3$, $n = 5$).

(0.1–1000 μM), measured the associated intracellular elevation of IP_3 and probed the effect of IP3RPEP6 (5 different concentrations in the 10–1000 μM range) on the induced $[Ca^{2+}]_i$ responses. Figure 3A illustrates that increasing concentrations of IP3RPEP6 necessitated larger IP_3 elevation to obtain the same degree of $[Ca^{2+}]_i$ increase as observed without the peptide, indicating IP_3 competes with the peptide for access to the IP_3R ligand-binding domain.

Next, we performed control experiments on RyRs to test possible IP3RPEP6 effects on this other major ER Ca^{2+}-release channel, making use of an inducible RyR2 overexpression HEK cell model[50] (Figure 3B). Application of a high intracellular IP3RPEP6 concentration (~64 μM, electroporation loaded) had no significant effect on the amplitude and duration of caffeine-induced $[Ca^{2+}]_i$ transients in HEK-RyR2 cells (Figure 3C–E).

2.5 | Carbachol-induced $[Ca^{2+}]_i$ responses in HEK cells involve a Cx43 hemichannel contribution

Cx43 hemichannel opening allows substantial Ca^{2+} entry due to the high (220–240 pS) single-channel conductance, providing ~1–1.5 pA Ca^{2+} current per hemichannel at −70 mV membrane potential.[32,51] As many cell types show background Cx43 expression, we verified whether carbachol-induced $[Ca^{2+}]_i$ changes were affected by

17481716, 0, Downloaded from https://onlinelibrary.wiley.com/doi/10.1111/apha.14086 by Ku Leuven, Wiley Online Library on [02/02/2024]. See the Terms and Conditions (https://onlinelibrary.wiley.com/terms-and-conditions) on Wiley Online Library for rules of use; OA articles are governed by the applicable Creative Commons License

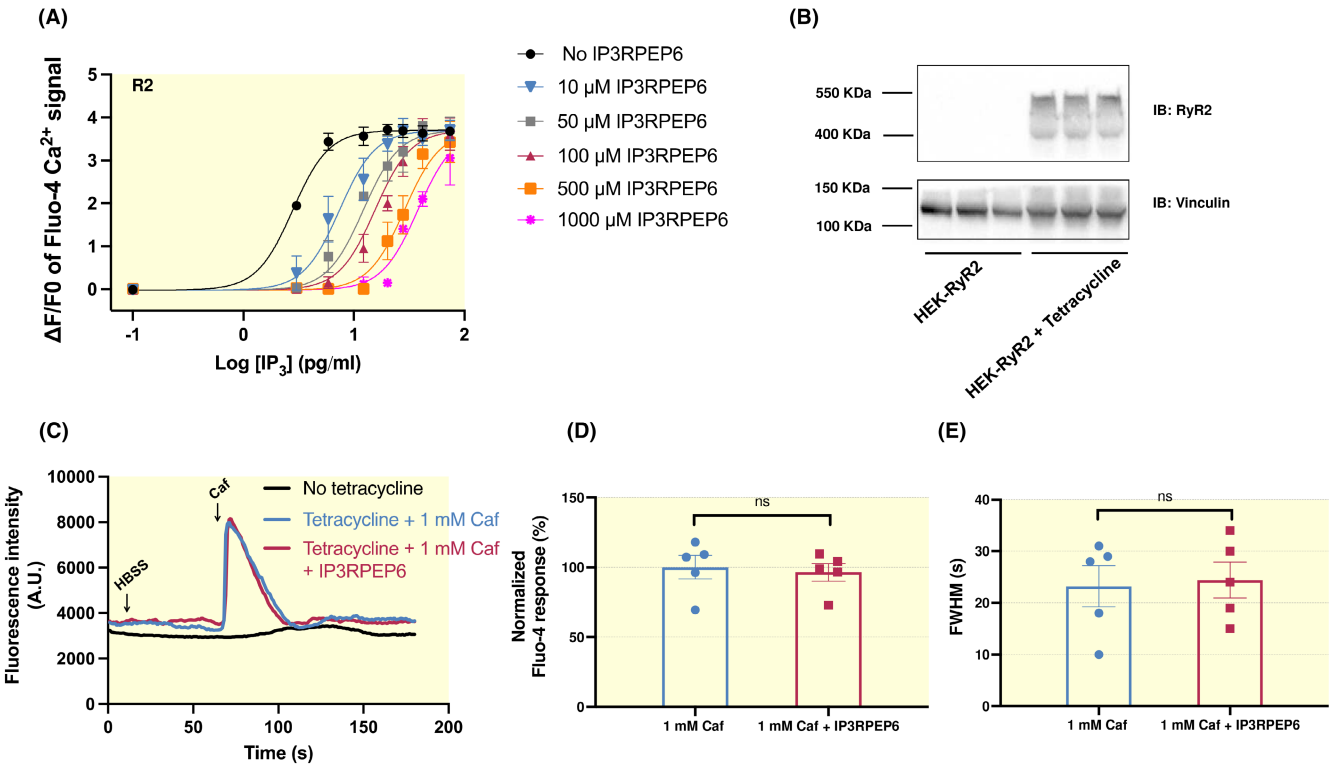

FIGURE 3 IP3RPEP6 acts as a competitive antagonist of IP_3R2. (A) Concentration-dependent carbachol-induced IP_3 elevation and cellular Ca^{2+} response curves are right-shifted by increasing concentrations of IP3RPEP6, indicating IP_3 competes with the peptide for access to the IP_3 receptor ($N = 3$, $n = 5$). (B) Western blotting showing tetracycline-induced RyR2 protein overexpression in HEK cell lysates. The second ~400 kDa RyR2 band corresponds to a C-terminal fraction of the channel.[84,85] Vinculin was used as a loading control; 20 μg lysate was loaded per lane (IB: immunoblot). (C) Representative traces of caffeine-induced Ca^{2+} changes (1 mM caffeine) in HEK-RyR2 cells in the absence and presence of tetracycline. (D, E) Summary data demonstrating no effect of ~60 μM IP3RPEP6 on the amplitude and duration (FWHM, full-width at half-maximum) of the caffeine-induced Ca^{2+} transients ($N = 5$, $n = 5$; unpaired Student's *t*-test). Data are expressed as the mean ± SEM.

inhibiting Cx43 hemichannels using Gap19, which selectively targets Cx43-based hemichannels without inhibiting Cx43 gap junctions.[52] We first recorded $[Ca^{2+}]_i$ responses to carbachol in HEK-WT cells and HEK cells transduced with Cx43.[53] Immunoblot Cx43 staining revealed a clear Cx43 band in HEK-WT, indicating endogenous Cx43 expression; Cx43 protein levels were about fivefold higher in HEK-Cx43 cells (Figure S5A,B). HEK cells furthermore displayed low background expression of Cx45 and were negative for Cx37 and Cx40 (Figures S5C,D). Figure 4A,B illustrate typical $[Ca^{2+}]_i$ traces recorded in both cell types, demonstrating larger $[Ca^{2+}]_i$ peaks in HEK-Cx43 cells compared to HEK-WT (~37% larger—see Figure 4C,D). The EC_{50} was also different, being lower (1.53 μM) in HEK-Cx43 compared to HEK-WT (2.58 μM). Strikingly, Gap19 inhibition reduced the $[Ca^{2+}]_i$ response amplitude in HEK-Cx43 cells and increased the EC_{50} from 1.53 to 6.56 μM (~4 times increase) and the Hill slope from 0.87 to 1.94 (Figure 4D). A similar effect was observed in HEK-WT, most clearly for the EC_{50} that increased from 2.58 to 6.37 μM (Figure 4C).

2.6 | IP3RPEP6 inhibition of carbachol-triggered $[Ca^{2+}]_i$ responses is modified by the presence of Cx43

Figure 4E,F demonstrate that concentration-dependent inhibition by IP3RPEP6 was very different between WT and Cx43 overexpressing cells (submaximal carbachol stimulation, as in Figure 2G–I). In HEK-WT, the IP3RPEP6 inhibition curve had a high IC_{50} (7.4 μM) and a low negative Hill slope (1.3) (Figure 4E), while HEK-Cx43 cells had a lower IC_{50} (5.2 μM) and a very steep negative Hill slope (3.1) (Figure 4F). Because the HEK-WT curve (Figure 4E) appeared similar to the HEK-IP_3R1 curve (Figure 2G) while the HEK-Cx43 curve (Figure 4F) more closely resembled inhibition as observed for IP_3R2 and IP_3R3 (Figure 2H,I), we checked IP_3R-protein levels in HEK-WT and HEK-Cx43 cells using isoform-selective antibodies. This demonstrated 2.4-fold larger IP_3R3 protein levels in HEK-Cx43 compared to WT (Figure S6), while there were no significant differences in the protein levels of IP_3R1 and IP_3R2. This larger expression of IP_3R3,

17481716, 0, Downloaded from https://onlinelibrary.wiley.com/doi/10.1111/apha.14086 by Ku Leuven, Wiley Online Library on [02/02/2024]. See the Terms and Conditions (https://onlinelibrary.wiley.com/terms-and-conditions) on Wiley Online Library for rules of use; OA articles are governed by the applicable Creative Commons License

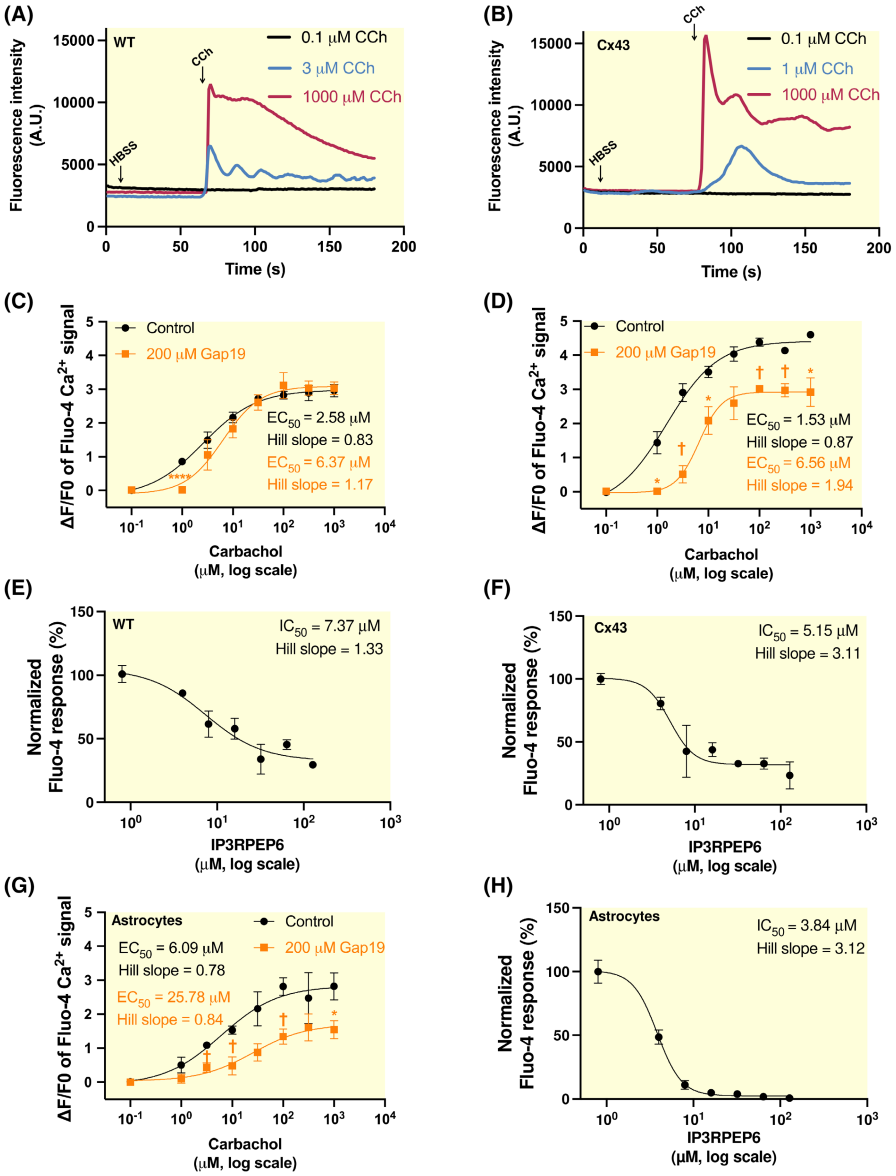

FIGURE 4 Cx43 hemichannels enhance carbachol-evoked Ca^{2+} transients and alter activation curve properties. Panels A and B show representative carbachol-triggered Ca^{2+} transients in HEK-WT and HEK-Cx43 cells, respectively, while C and D summarize concentration-response curves derived from such experiments. The orange curves indicate carbachol-induced cytoplasmic Ca^{2+} changes in the presence of Gap19 (200 μM) in HEK-WT and HEK-Cx43 cells ($N = 3$, $n = 5$; $^{*}p < 0.05$, $^{\dagger}p < 0.01$, $^{****}p < 0.0001$ versus control; unpaired Student's *t*-test). Panels E and F demonstrate concentration-dependent inhibition of carbachol-induced Ca^{2+} elevation by IP3RPEP6 in HEK-WT and Cx43 overexpressing HEK cells. (G) Concentration-response curves for carbachol-induced cytoplasmic Ca^{2+} changes in the absence or presence of Gap19 (200 μM) in astrocytes ($N = 3$, $n = 5$; $^{*}p < 0.05$, $^{\dagger}p < 0.01$ versus control; unpaired Student's *t*-test). (H) Concentration-dependent inhibition of carbachol-induced Ca^{2+} elevation by IP3RPEP6 in astrocytes ($N = 3$, $n = 5$). Data are normalized to control responses without peptide and expressed as mean ± SEM.

which displays a steep Hill slope for IP3RPEP6 inhibition (Figure 2I), could in part explain the steeper Hill slope for IP3RPEP6 inhibition in HEK-Cx43 relative to HEK-WT (compare Figure 4E,F). Inhibition at high IP3RPEP6 concentration was incomplete in HEK-WT and HEK-Cx43 (Figure 4E,F), as observed in HEK-IP_3R1 cells (Figure 2G) indicating this is linked to IP_3R1.

2.7 | IP3RPEP6 dose-dependently inhibits carbachol-triggered $[Ca^{2+}]_i$ elevations in astrocytes isolated from mouse brain

Astrocytes highly express Cx43, necessary to sustain spatial K^+ buffering.[54] We used primary cultures of mouse brain astrocytes to determine the effect of IP3RPEP6 on carbachol-induced $[Ca^{2+}]_i$ transients in these endogenously Cx43-expressing cells. Figure S5 illustrates astrocytic Cx43 expression relative to the expression in the other cells used in this study. Carbachol-evoked $[Ca^{2+}]_i$ responses were characterized by an EC_{50} of 6.09 μM (Figure 4G). As observed for HEK-Cx43 cells, Gap19 strongly reduced the amplitude of the carbachol-induced $[Ca^{2+}]_i$ changes and quadrupled the EC_{50} for Ca^{2+} response activation from 6.09 to 25.78 μM, while leaving the Hill slope unaffected (Figure 4G). Figure 4H illustrates the effect of IP3RPEP6 on the astrocytic Ca^{2+} responses, which were characterized by an IC_{50} of 3.84 μM and a negative Hill slope of ~3, very similar to the observations in HEK-IP_3R2 cells (Figure 2H). Astrocytic Ca^{2+} responses were completely inhibited by 10 μM IP3RPEP6 and above (Figure 4H), which differs from the responses in HEK-Cx43 (Figure 4F). Immunoblotting revealed high IP_3R1 and IP_3R2 protein levels in astrocytes (Figure S6), in line with previous reports.[55] Thus, in astrocytes expressing both IP_3R1 and IP_3R2, inhibition by

17481716, 0, Downloaded from https://onlinelibrary.wiley.com/doi/10.1111/apha.14086 by Ku Leuven, Wiley Online Library on [02/02/2024]. See the Terms and Conditions (https://onlinelibrary.wiley.com/terms-and-conditions) on Wiley Online Library for rules of use; OA articles are governed by the applicable Creative Commons License

IP3RPEP6 was complete while IP3RPEP6 inhibition in HEK-IP_3R1 was incomplete (Figure 2G) and complete in HEK-IP_3R2 (Figure 2H). Full inhibition by IP3RPEP6 in astrocytes may result from the fact that IP_3R2 dominates the Ca^{2+} responses in these cells. IP_3R2 is expressed in the astrocytic soma and major branches while IP_3R1 mainly locates in peri-synaptic extensions therefore having a minor contribution to the global signal.[55–57] A further scrutiny of CCh-triggered Ca^{2+} responses in astrocytes, HEK-WT and HEK-Cx43 cells is given in Figure S7.

2.8 | IP3RPEP6 binds to IP_3R2 in HEK IP_3R2, HEK Cx43 and brain astrocytes

We determined whether IP3RPEP6 could directly interact with IP_3Rs, using biotin-conjugated IP3RPEP6 and pull-down assays with Neutravidin-coated beads and lysates prepared from HEK-IP_3R2, HEK-Cx43 and brain astrocytes. Affinity-purified samples were analyzed via immunoblotting and stained for the three IP_3R isoforms to assess isoform-specific IP3RPEP6 binding (Figure 5). IP3RPEP6 was able to pull down IP_3R2 in cell lysates from HEK-IP_3R2, from HEK-Cx43 and from primary astrocytes (Figure 5B). The observed biotin-IP3RPEP6/IP_3R2 interaction was specific as non-active biotin-conjugated IP3RPEP6-E4K was unable to pull down IP_3R2 from lysates. IP3RPEP6 also interacted with IP_3R3 from HEK-Cx43 cell lysates but with lower efficiency compared to IP_3R2 (Figure 5C). In astrocyte lysates, no IP_3R3 could be detected in biotin-IP3RPEP6-pull-down samples, most likely because of the low IP_3R3-protein levels in these samples. Biotin-IP3RPEP6 failed to pull down IP_3R1 in lysates from HEK-Cx43 cells and astrocytes (Figure 5A). These IP3RPEP6/IP_3R-isoform interactions underpin the functional results of isoform-specific IP_3R inhibition by IP3RPEP6, indicating IP3RPEP6 displays higher affinity for $IP_3R2/3$ than for IP_3R1.

2.9 | IP3RPEP6 inhibits IP_3-induced Cx43 hemichannel opening in HeLa cells

As the IP_3/Ca^{2+}-signaling axis is a strong activator of Cx43 hemichannel opening,[31,58,59] we further investigated whether IP3RPEP6 could inhibit IP_3-triggered hemichannel opening. We used UV-photoactivation of caged-IP_3 and recorded Cx43 hemichannel activity in whole-cell patch-clamp experiments on HeLa-Cx43 cells. Hemichannel currents were activated by voltage steps from −30 to +70 mV, which triggered single-channel current activity with a unitary conductance of ~240 pS typical for Cx43 hemichannels (Figure 6A,B). Uncaging IP_3 (caged-IP_3, 10 μM in pipette)

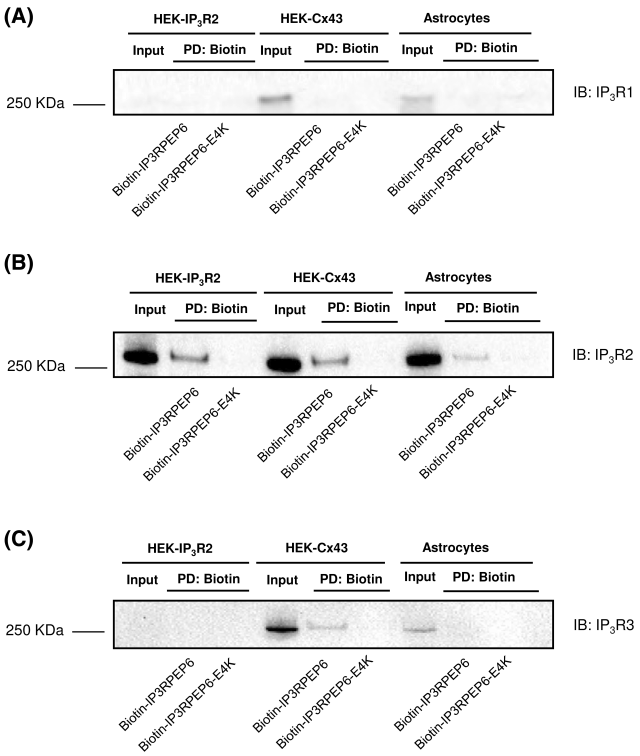

FIGURE 5 IP3RPEP6 binds to IP_3R2 in HEK IP_3R2 cells, HEK Cx43 cells and astrocytes. Representative Biotin-pull-down experiments using Neutravidin-coated beads assessing the binding of IP_3R1 (A), IP_3R2 (B) and IP_3R3 (C) to immobilized biotin-IP3RPEP6 using lysates obtained from HEK-IP_3R2, HEK-Cx43 and astrocytes. This experiment was performed three times using each time freshly prepared cell lysates. Biotin-IP3RPEP6-E4K served as negative control to determine the level of non-specific binding. The samples were analyzed by immunoblotting using isoform-specific Abs against IP_3Rs; total cell lysate was used as input (10 μg). IB, immunoblot; PD, pull-down. The corresponding western blotting for Biotin-IP3RPEP6 and Biotin-IP3RPEP6-E4K is shown in Figure S8A–C. Empty NeutrAvidin beads, added as a negative control are shown in Figure S8D.

significantly increased unitary event activity quantified by membrane charge transfer (Q_m), as illustrated in Figure 6C. The increased Cx43 hemichannel activity was reduced to control level by IP3RPEP6 (50 μM in pipette) without affecting the unitary conductance (Figure 6C). We further characterized concentration-dependent effects of IP3RPEP6 on hemichannel ATP-release from HeLa-Cx43 cells triggered by IP_3-uncaging/Ca^{2+} signaling. IP_3-triggered ATP-release was dependent on the concentration of caged-IP_3 loaded by electroporation[47] (Figure 6D) and was inhibited by 5 μM Xestospongin C (Figure 6E). Moreover, IP3RPEP6 concentration-dependently inhibited ATP-release with an IC_{50} of ~8.6 μM and a negative Hill slope of 2.8 (Figure 6F), while the control peptide IP3RPEP6-E2A had no effect (Figure S2C).

17481716, 0, Downloaded from https://onlinelibrary.wiley.com/doi/10.1111/apha.14086 by Ku Leuven, Wiley Online Library on [02/02/2024]. See the Terms and Conditions (https://onlinelibrary.wiley.com/terms-and-conditions) on Wiley Online Library for rules of use; OA articles are governed by the applicable Creative Commons License

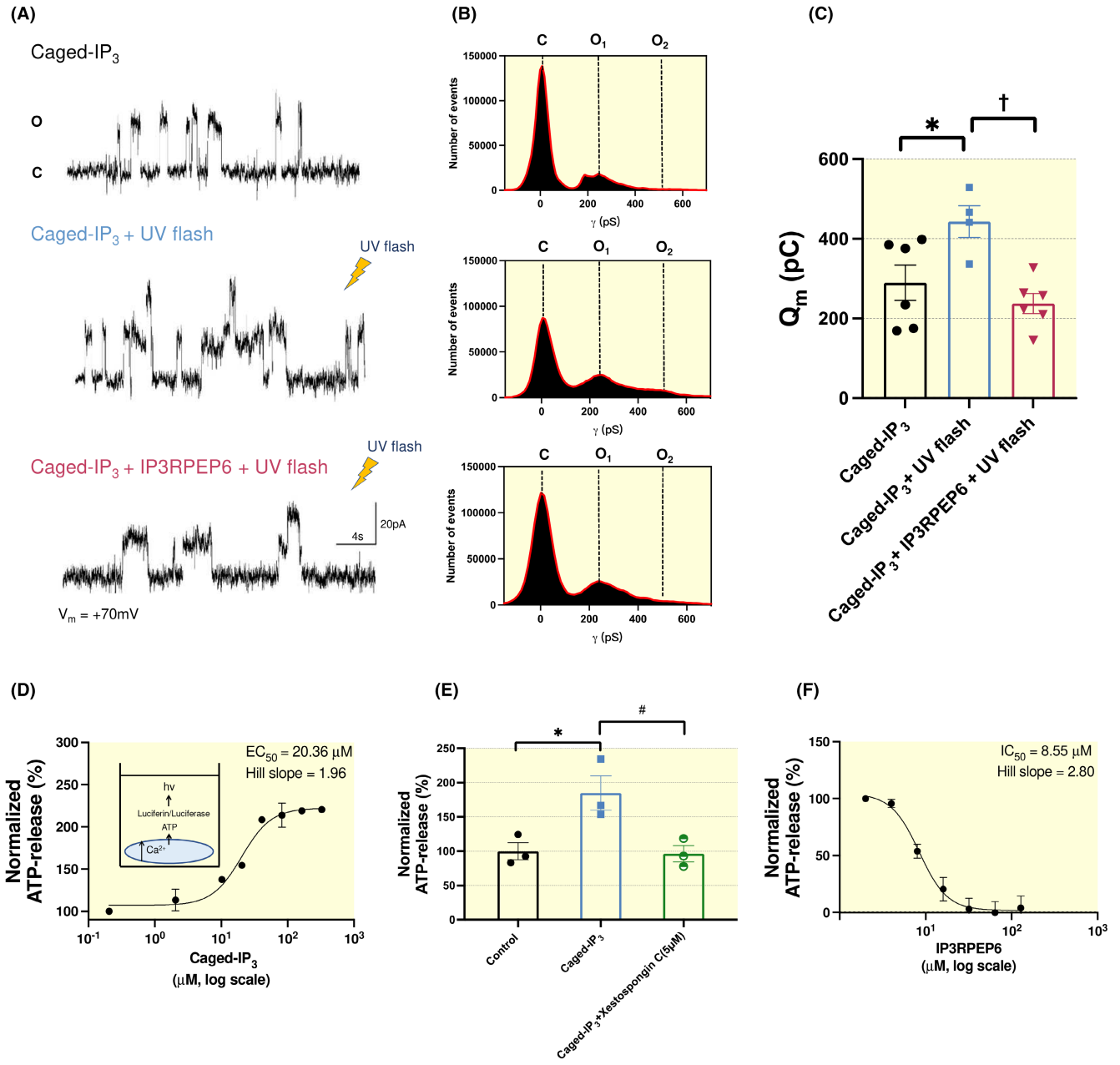

FIGURE 6 IP3RPEP6 inhibits Cx43-hemichannel opening evoked by IP_3. (A) Representative current traces recorded in HeLa-Cx43 cells evoked by stepping V_m from −30 mV to +70 mV for 30 s to provoke electrically triggered Cx43 hemichannel activity in whole-cell recording mode. The first trace marked "caged-IP_3" demonstrates a control response with caged-IP_3 loaded into the cell through the pipette (10 μM) without UV exposure. In the second trace, uncaging was induced by application of the UV flash at the start of the voltage step, resulting in increased Cx43 hemichannel opening discernable from, for example, "stacked" openings (opening of a second hemichannel superimposed on an already open hemichannel). The third trace was as the second trace but with IP3RPEP6 added to the pipette solution (50 μM). (B) All-point histograms of experimental recordings as illustrated in panel A expressed as event counts as a function of the conductance. Control conditions are characterized by a large peak of the closed state ("C") and some activity at the 240 pS single channel unitary conductance level (O_1 level) that is within the typical range for Cx43 hemichannels. Uncaging IP_3 reduced the frequency of the closed state and extended the distribution towards the O_2 level (480 pS), while in the presence of IP3RPEP6, the distribution appeared similar to control conditions. (C) Summary data of membrane charge transfer Q_m, illustrating significant inhibition by IP3RPEP6 (caged-IP_3, $N=6$, $n=3$; caged-IP_3 + UV flash, $N=4$, $n=4$; caged-IP_3 + IP3RPEP6 + UV flash, $N=6$, $n=3$; $^*p<0.05$ versus control, $^\dagger p<0.01$ versus caged-IP_3 + UV flash; one-way ANOVA, Dunnett post-test). (D) Experiments in HeLa-Cx43 cells illustrating ATP-release triggered by IP_3 uncaging as a function of caged-IP_3 concentration loaded into the cells by electroporation ($N=3$, $n=3$; caged IP_3 concentration represents intracellular concentration before flash; flashes released 5%–10% as IP_3). (E) Xestospongin C (5 μM, added 15 min before IP_3 uncaging) significantly inhibited the ATP-release ($N=3$, $n=3$; $^*p<0.05$ versus control, $^\#p<0.05$ versus caged IP_3; one-way ANOVA, Dunnett post-test). (F) Concentration-dependent inhibition of the responses by IP3RPEP6 ($N=3$, $n=3$). Data are expressed as the mean ± SEM.

17481716, 0, Downloaded from https://onlinelibrary.wiley.com/doi/10.1111/apha.14086 by Ku Leuven, Wiley Online Library on [02/02/2024]. See the Terms and Conditions (https://onlinelibrary.wiley.com/terms-and-conditions) on Wiley Online Library for rules of use; OA articles are governed by the applicable Creative Commons License

2.10 | IP3RPEP6 does not affect Cx43 hemichannel opening

We verified whether IP3RPEP6 had intrinsic effects on Cx43 hemichannels using HEK-TKO cells, in which the IP_3-Ca^{2+} signaling axis was silenced (Figure S2A); these cells displayed Cx43 expression slightly (but non-significantly) above the level of HEK-IP_3R1, 2 and 3 (Figure S5). We activated hemichannel opening by challenging the cells with a low Ca^{2+} bath solution by addition of 4 mM EGTA to the standard bath solution.[60–62] Challenging HEK-TKO cells with low extracellular Ca^{2+} triggered extracellular ATP-release that was completely inhibited by 200 μM extracellular Gap19, demonstrating that ATP-release proceeded via Cx43 hemichannels (Figure 7A). We subsequently found that intracellular IP3RPEP6 (tested up to 300 μM, electroporation loaded) had no effect on ATP-release, demonstrating that the peptide did not affect hemichannels (Figure 7B).

We further used HEK-TKO cells to test 2-APB, known to affect several non-IP_3 receptor targets (Table S1). Figure 7B illustrates that 2-APB inhibited hemichannel ATP responses in a concentration-dependent manner with an IC_{50} of ~20.5 μM. Application of Xestospongin C at the commonly used concentration of 5 μM showed no significant effects (Figure 7C).

2.11 | Blocking Cx43 hemichannels with Gap19 does not affect Ca^{2+} responses in HEK IP_3R2 cells

Hemichannel opening increases the amplitude of carbachol-induced $[Ca^{2+}]_i$ transients (see Gap19 effect in Figure 4D). Therefore, the concentration-dependent effect of IP3RPEP6 on carbachol-induced $[Ca^{2+}]_i$ transients (Figure 2G–I) may also be affected by background Cx43 expression and hemichannel opening. To verify this, we

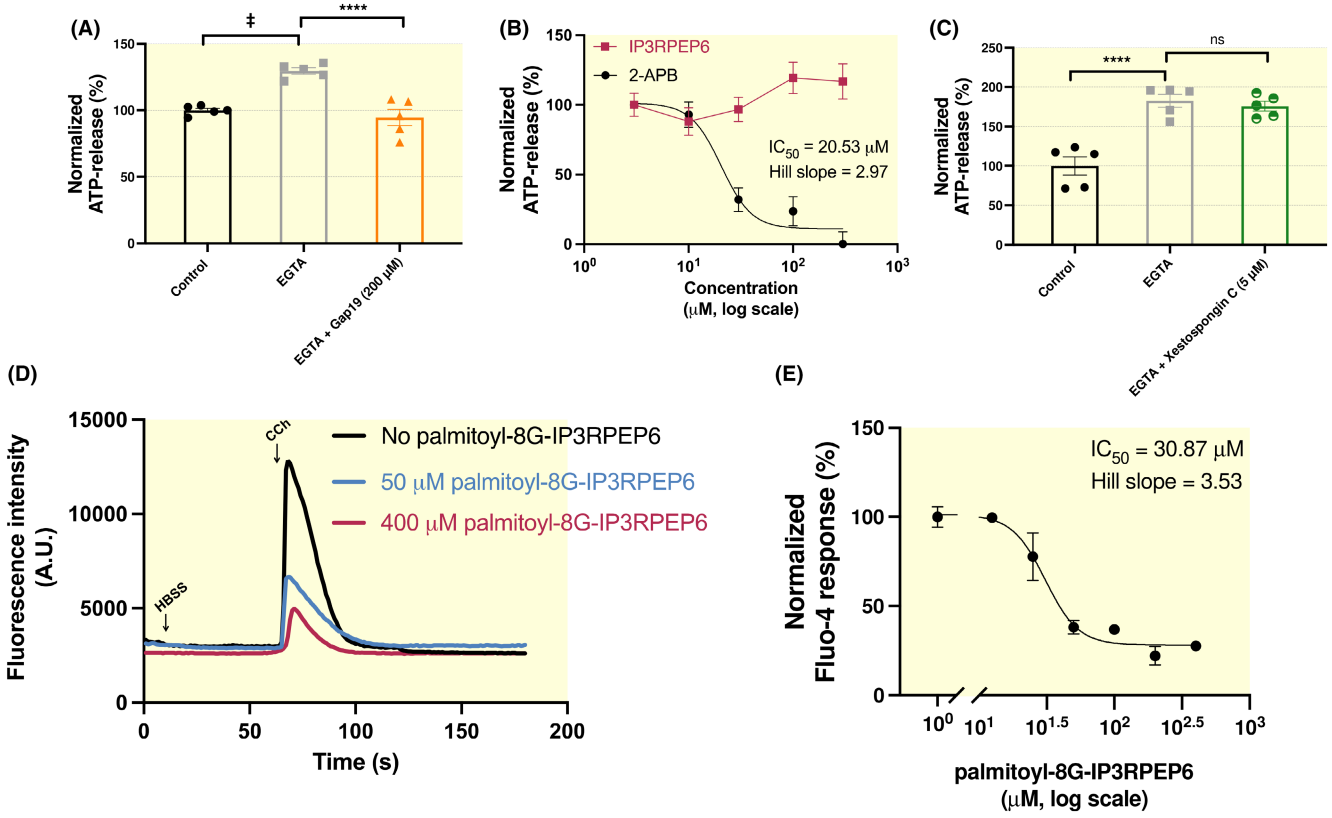

FIGURE 7 2-APB inhibits low extracellular Ca^{2+} triggered Cx43 hemichannel opening. (A) ATP-release triggered by exposure of HEK-TKO cells to low extracellular Ca^{2+} (EGTA) was reduced to baseline level by 200 μM Gap19 ($^{‡}p < 0.001$ versus control, $^{****}p < 0.0001$ versus EGTA; one-way ANOVA, Dunnett post-test), confirming the response is mediated by hemichannels. ATP-release expressed relative to 100% baseline signal ($N = 5$, $n = 3$). (B) 2-APB concentration-dependently inhibited the ATP response with an IC_{50} of 20.5 μM (ATP-release expressed relative to 100% EGTA stimulation; $N = 5$, $n = 3$) while electroporation-loaded IP3RPEP6 had no significant effects over the 3–300 μM range. (C) Xestospongin C applied at 5 μM had no significant effect ($N = 5$, $n = 3$; $^{****}p < 0.0001$ versus control; one-way ANOVA, Dunnett post-test). (D) Representative Ca^{2+} traces in control and in the presence of palmitoyl-8G-IP3RPEP6 in HEK-IP_3R2 cells. (E) Concentration-dependent inhibition of carbachol-induced Ca^{2+} elevation by palmitoyl-8G-IP3RPEP6 in HEK-IP_3R2 cells ($N = 3$, $n = 5$). Data are expressed as the mean ± SEM.

17481716, 0, Downloaded from https://onlinelibrary.wiley.com/doi/10.1111/apha.14086 by Ku Leuven, Wiley Online Library on [02/02/2024]. See the Terms and Conditions (https://onlinelibrary.wiley.com/terms-and-conditions) on Wiley Online Library for rules of use; OA articles are governed by the applicable Creative Commons License

recorded carbachol-induced $[Ca^{2+}]_i$ responses in HEK-IP_3R2 cells in the presence of 200 μM Gap19. Figure S9A demonstrates a slight but non-significant increase in the IC_{50} of IP3RPEP6 in the presence of Gap19 hemichannel block, indicating non-significant contribution of Cx43 hemichannel activity to the responses in these cells.

2.12 | Extracellularly applied palmitoyl-8G-IP3RPEP6 inhibits IP_3R2 Ca^{2+} responses

We tested N-terminal addition of a palmitoyl group to IP3RPEP6 to facilitate membrane permeability and allow extracellular application. To increase flexibility of the active IP3RPEP6 moiety relative to the palmitate part, we included 8 Gly residues between the peptide and the palmitoyl group yielding palmitoyl-8G-IP3RPEP6. Extracellular application of palmitoyl-8G-IP3RPEP6 provided concentration-dependent inhibition of carbachol-induced $[Ca^{2+}]_i$ responses, characterized by an IC_{50} of ~30 μM (1 h peptide incubation). The negative Hill slope was slightly steeper than for IP3RPEP6; maximal inhibition at high concentration was 72% (Figure 7D,E). In contrast, conjugation with the TAT cell-permeation sequence (YGRKKRRQRRR) did not confer any inhibition upon extracellular application (Figure S9B), possibly due to interaction between the positively charged TAT sequence and the negatively charged IP3RPEP6 moiety rendering the peptide inactive.

3 | DISCUSSION

Currently, there are few effective and selective IP_3R antagonists,[13] with none of them being free of pitfalls.[63] Commonly used IP_3R antagonists, such as heparin, 2-APB, caffeine and Xestospongins, lack subtype-selectivity and affect other targets[18] (Table S1). For example, 2-APB also blocks gap junctions with IC_{50} concentrations depending on the isotype (IC_{50} of ~50 μM for Cx43 while ~3 μM for the neuronal Cx36).[64] Here, we found 2-APB to inhibit Cx43-based hemichannels with an IC_{50} of ~20 μM (Figure 7B), that is, 2.5-fold lower than for gap junctions. Inspired by the recent identification of a self-binding sequence in IP_3R3 (Figure 1A), we conceived and characterized IP3RPEP6 consisting of an IP_3R2-based sequence that competitively interacts with IP_3 binding to the receptor site. We found the peptide to interact with IP_3R2 in HEK-IP_3R2 cells, HEK-Cx43 cells and astrocytes (Figure 5) and with IP_3R3 in HEK-Cx43 cells. Interaction with IP_3R1 was absent in both astrocytes and HEK-Cx43 cells, suggesting an IP3RPEP6 interaction order of $IP_3R2 > IP_3R3 > IP_3R1$. At the single-channel level, IP3RPEP6 concentration-dependently reduced the open probability of IP_3R2 channels (Figure 1E). At the functional signaling level, IP3RPEP6 inhibition of carbachol-triggered $[Ca^{2+}]_i$ responses suggested a potency order of $IP_3R2 \approx IP_3R3 < IP_3R1$. Inhibition of IP_3R2 and IP_3R3 was complete while incomplete for IP_3R1 (Figure 2G–I). At a 5.5 μM concentration, IP3RPEP6 inhibited IP_3R1 less than ⅓, IP_3R2 for ¾ and IP_3R3 for ⅔ while not affecting RyR2 (Figure 3C–E). With Gap19 hemichannel block, 5.5 μM IP3RPEP6 gave ~⅔ inhibition of IP_3R2 compared to ¾ inhibition without Gap19. This smaller degree of IP3RPEP6 inhibition in the presence of Gap19 is caused by the removal of the hemichannel contribution to the $[Ca^{2+}]_i$ response amplitude, making the control responses smaller to start with (and therefore relatively less inhibited). The Gap19 effect-size will depend on the cellular Cx43 expression level (compare Figure 4C with D,G). As IP3RPEP6 inhibition is competitive, the concentration values given above only apply to the carbachol stimulation used here and may vary with IP_3 levels associated with other stimulation protocols.

Our work demonstrates that IP_3-signaling enhances opening of hemichannels composed of Cx43, a ubiquitously expressed connexin isotype abundantly present in astrocytes and cardiomyocytes. Cx43 hemichannel opening results in Ca^{2+} entry amounting to 1–1.5 pA Ca^{2+} current per hemichannel at −70 mV membrane potential,[32] a typical resting potential for astrocytes and cardiomyocytes. In cardiomyocytes, this may increase $[Ca^{2+}]_i$ in subplasmalemmal microdomains to the 1–4 μM range per single open hemichannel.[32] Hemichannel opening also results in the release of ATP, which is known to activate purinergic receptors, inducing Ca^{2+} entry and IP_3-triggered Ca^{2+} release.[27,65] In both cases, Gap19-mediated inhibition of Cx43 hemichannel opening will impact the $[Ca^{2+}]_i$ responses as shown here. Consequently, the IC_{50}, Hill slope and maximal inhibition properties of IP_3R inhibitors will be affected by hemichannel contributions to the Ca^{2+} signal, which can be verified by recording these pharmacological properties under control conditions and in the presence of Cx43 hemichannel block by Gap19, as demonstrated in Figure 4C,D,G.

Astrocytes are a major glial brain cell type predominantly expressing IP_3R1 and IP_3R2 (Figure S6),[55] with high endogenous Cx43 expression (Figure S5).[66,67] Interestingly, IP3RPEP6 inhibition of astrocytic $[Ca^{2+}]_i$ responses (Figure 4H) displayed similar IC_{50} and Hill slope properties as for HEK-IP_3R2 (Figure 2H). Remarkably, IP3RPEP6 inhibition in HEK-IP_3R1 and HEK-Cx43 was incomplete at high peptide concentrations, while complete in astrocytes expressing IP_3R1 and Cx43, which may be related to functional dominance of IP_3R2 in astrocytes,[55–57]

17481716, 0, Downloaded from https://onlinelibrary.wiley.com/doi/10.1111/apha.14086 by Ku Leuven, Wiley Online Library on [02/02/2024]. See the Terms and Conditions (https://onlinelibrary.wiley.com/terms-and-conditions) on Wiley Online Library for rules of use; OA articles are governed by the applicable Creative Commons License

consistent with its highest affinity for IP_3 among the three distinct IP_3R isoforms. IP_3R2 is furthermore important in cellular Ca^{2+} waves and oscillations,[68] while IP_3R1 has not been observed to participate in such dynamic Ca^{2+} responses in astrocytes.[69,70] In line with this, astrocytic ER stores seem to be more heterogeneous allowing independent subcompartment release of Ca^{2+}.[71]

In conclusion, IP3RPEP6 is a novel competitive peptide antagonist of $IP_3R2/3$ with limited effects on IP_3R1 at ~5.5 μM and submaximal effects on $IP_3R2/3$ at 10 μM associated with half-maximal inhibition of IP_3R1; its membrane permeable version palmitoyl-8G-IP3RPEP6 requires ~7.5 times higher concentrations for IP_3R2 inhibition. Importantly, the peptide does not inhibit RyR2 or Cx43 hemichannels. Hemichannels open as a consequence of IP_3/Ca^{2+} signaling and increase the amplitude of the $[Ca^{2+}]_i$ responses. Consequently, IP_3-dependent cellular $[Ca^{2+}]_i$ responses should be verified for hemichannel-linked Ca^{2+} contributions that modify the amplitude and dynamics of the responses as recently demonstrated for cytokine-induced Ca^{2+} oscillations, for example.[72]

4 | MATERIALS AND METHODS

4.1 | Chemical reagents

Carbachol, caffeine, tetracycline and 2-aminoethoxydiphenyl borate (2-APB) were purchased from Sigma-Aldrich (Bornem, Belgium). Caged-IP_3 was from Sichem (Bremen, Germany). Fluo-4-AM, Mag-Fluo-4-AM and Pierce™ NeutrAvidin™ Agarose were from Molecular Probes (Invitrogen, Merelbeke, Belgium). IP3RPEP6, its inactive versions IP3RPEP6-E2A and IP3RPEP6-E4K and its membrane-permeable version palmitoyl-8G-IP3RPEP6 were from GenScript Biotech (Netherlands). All peptides were synthesized to a purity >95% by HPLC analysis and correct mass spectrometry-controlled molecular weight.

4.2 | Cell culture

HEK cells, in which CRISPR/Cas9 was used to delete one or more IP_3R subtypes (RRID:CVCL_UR28), were generated by Dr. David Yule's laboratory (University of Rochester, NY)[46] and supplied by Kerafast. The HEK (HEK-293) and HEK-Cx43 cell lines were cultured in Dulbecco's Modified Eagle's Medium (DMEM) (Invitrogen, Gent, Belgium) supplemented with foetal bovine serum (FBS, 10%), 10 U mL^{-1} penicillin, 10 μg mL^{-1} streptomycin (Invitrogen, Gent, Belgium). For tetracyclin-inducible RyR2 expression, we used modified HEK-293 cells kindly provided by Dr. S.R. Wayne Chen.[50] These cells were cultured in Dulbecco's Modified Eagle's Medium (DMEM) (Invitrogen, Gent, Belgium) supplemented with foetal bovine serum (FBS, 10%), 10 U mL^{-1} penicillin, 10 μg mL^{-1} streptomycin, 0.1 mM minimum Eagle's medium nonessential amino acids (Invitrogen, Gent, Belgium); 1 μg mL^{-1} tetracycline was applied 18–24 h before functional assays to induce RyR2 expression. HeLa cells stably transfected with Cx43 were grown in Dulbecco's Modified Eagle's Medium (DMEM)/F-12 (Invitrogen, Gent, Belgium) supplemented with foetal bovine serum (FBS, 10%), 10 U mL^{-1} penicillin, 10 μg mL^{-1} streptomycin (Invitrogen, Gent, Belgium) with additional 1 μg mL^{-1} puromycin (Sigma-Aldrich, Bornem, Belgium) to ensure a stable Cx43 expression. All cells above were maintained at 37°C in humidified air with 5% CO_2, and passaged every 3–4 days.

DT40 cells lacking all three IP_3R isoforms (DT40-TKO) (RCB Cat# RCB1467, RRID:CVCL_4634) heterologously expressing IP_3R2 were used for the on-nucleus patch-clamp experiments.[46,73,74] The cells were cultured at 39°C in humidified air with 5% CO_2 in RPMI 1640 medium supplemented with 10% foetal bovine serum (FBS), 1% chicken serum, 2.05 mM L-glutamine, 50 μM 2-mercaptoethanol, 2 mg mL^{-1} G418 sulfate, 100 U mL^{-1} penicillin and 100 μg mL^{-1} streptomycin. RPMI 1640 medium, penicillin/streptomycin, G418 sulfate, 2-mercaptoethanol and chicken serum were purchased from Invitrogen. Foetal bovine serum was from Gemini Bio-products.

4.3 | Astrocyte isolation

Astrocytes were isolated from early postnatal (P3–P4) mouse cortices (C57BL/6) as previously described.[75,76] Dissected cortices were triturated in DMEM/F-12 (Invitrogen, Gent, Belgium) and then seeded into flasks coated with 0.01% solution poly-L-Lysine (Sigma-Aldrich) (four cortices per T75 flask). Culture media (DMEM/F-12 supplemented with 10% FBS, 10 U mL^{-1} penicillin and 10 μg mL^{-1} streptomycin) was replaced 4 h after plating and every second day thereafter. After 7 to 8 days, oligodendrocytes formed different layers, and the separation of astrocytes from oligodendrocytes and microglia was achieved by shaking the tissue culture flask on an orbital shaker. Astrocytes were then harvested with trypsin–EDTA (Invitrogen, Gent, Belgium) and replated in a tissue culture flask.

4.4 | Peptide modeling and docking

A cryo-EM structure of the human type-3 inositol trisphosphate receptor reveals the presence of a self-binding

17481716, 0, Downloaded from https://onlinelibrary.wiley.com/doi/10.1111/apha.14086 by Ku Leuven, Wiley Online Library on [02/02/2024]. See the Terms and Conditions (https://onlinelibrary.wiley.com/terms-and-conditions) on Wiley Online Library for rules of use; OA articles are governed by the applicable Creative Commons License

peptide that acts as a competitive antagonist on the IP_3 binding site.[21] A loop extending from ARM2 between the α_{ARM2}-1 and α_{ARM2}-2 domain forms a peptide structure that occupies the IP_3-binding site and reduces the sensitivity of IP_3R3 to its physiological agonist IP_3. Microscale thermophoresis results showed that IP_3 affinity for the N-terminal domain was over sevenfold lower than for the ligand binding domain alone, and confirmed that IP_3R3 SBP competed against IP_3 binding.

Based on these data, we predicted the interactions between the human IP_3R2 and SBP by homology modeling and docking studies. A homology model of human IP_3R2 was built with Modeller using the following templates: rat IP_3R1 (PDB code 3JAV by Ref. [10]), rat IP_3R1 with adenophostin A (6MU1 by Ref. [77]), mouse IP_3R1 and mouse IP_3R1 with IP_3 (PDB codes 5XA0 and 5GUG by Ref. [11]). Homology modeling scores (molpdf, DOPE, GA341) and Ramachandran plot analysis were used to assess the model reliability.

4.5 | On-nucleus patch clamp experiments

Isolated nuclei from DT40-TKO cells stably expressing IP_3R2 were prepared by homogenization as previously described.[43] Single IP_3R channel potassium currents were measured in the on-nucleus patch clamp configuration using pCLAMP 9 and an Axopatch 200B amplifier (Molecular Devices, Sunnydale, CA, USA) as previously described.[78] Pipette solution contained 140 mM KCl, 10 mM HEPES, 100 μM BAPTA, 200 nM free Ca^{2+}, 1 μM IP_3, 5 mM ATP (pH 7.1). Free [Ca^{2+}] was calculated using Max Chelator software and verified fluorometrically. Traces were consecutive 3 s sweeps recorded at −100 mV, sampled at 20 kHz and filtered at 5 kHz.

4.6 | Electroporation loading of peptides

The IP3RPEP6 and related peptides used in this study have a limited membrane permeability and were therefore loaded into the cell monolayers by electroporation. We used 50 kHz AC electroporation that causes minimal cell damage/cell death as described before.[47–49] Cultures were briefly rinsed by a low-conductive electroporation solution consisting of (in mM) 300 sorbitol, 4.2 KH_2PO_4, 10.8 K_2HPO_4, 1 $MgCl_2$ and 2 HEPES, pH 7.2; thereafter the solution was removed leaving a thin layer just covering the cells. A bipolar electrode was positioned above the cells containing a small volume (7–9 μL) to which the peptides and/or caged IP_3 was added. The intracellular concentration of the peptides was determined from confocal imaging measurements with FITC-labeled peptides. For IP3RPEP6-FITC, the intracellular fluorescence was 16% of the fluorescence measured outside (Figure S3B).

4.7 | Calcium imaging

Intracellular cytoplasmic Ca^{2+} was monitored by epifluorescence microscopy and digital imaging using the Ca^{2+}-sensitive dye Fluo-4-AM. Cells were loaded with Fluo-4-AM by incubation for 1 h shielded from light at room temperature in HBSS-HEPES containing 10 μM Fluo-4-AM and Pluronic F-127 (final concentration 0.02%). Cultures were then washed with HBSS-HEPES and left at room temperature for 30 min for de-esterification. Carbachol was applied using a culture dish superfusion system. Images were captured using a Nikon TE300 inverted fluorescence microscope equipped with a 40× oil immersion objective (CFI S Fluor 40× oil, NA 1.30, Nikon) and an electron multiplying CCD camera (QuantEM 512SC EM CCD, Photometrics), recorded using Micro-Manager software (version 1.4.22) and analyzed using ImageJ software (rsbweb.nih.gov/ij). Calcium changes were expressed as relative fluorescence changes $\Delta F/F_0 = (F_t - F_0)/F_0$ (F_0 is the fluorescence before stimulation and F_t the time-dependent fluorescence signal after stimulation). The $\Delta F/F_0$ was calculated and analyzed with ImageJ software.

4.8 | Intracellular quantification of IP_3

Intracellular IP_3 was determined using a mouse IP_3 ELISA kit according to the protocols provided by the manufacturer (Antibodies-online GmbH, Aachen, Germany, Cat no. ABIN6974158).

4.9 | Caged-IP_3 loading and UV illumination

Caged-IP_3 (MW 635 Da) was loaded into the cells by electroporation; loading efficiency was determined by comparing the intracellular versus extracellular fluorescence signal (measured with a Leica TCS-SP8 confocal microscope) from several fluorescent probes including 6-carboxy fluorescein (6-CF, MW 376 Da), IP3RPEP6-FITC (MW 1651 Da) and 3 kDa dextran-FITC (MW 3389 Da), yielding an approximate 20% loading efficiency as concluded from interpolation (Figure S3C). UV illumination in the patch-clamp experiments (Figure 6A–C) was done with a 349 nm UV DPSS laser (Explorer, Spectra-Physics) connected to a fibre that was positioned close to the cell. UV illumination

17481716, 0, Downloaded from https://onlinelibrary.wiley.com/doi/10.1111/apha.14086 by Ku Leuven, Wiley Online Library on [02/02/2024]. See the Terms and Conditions (https://onlinelibrary.wiley.com/terms-and-conditions) on Wiley Online Library for rules of use; OA articles are governed by the applicable Creative Commons License

for the ATP-release experiments (Figure 6D–F) was done with a 100 W Hg-arc lamp with quartz collector lens and bandpass-filtered at 330 nm (330WB80, Omega Optical, Brattleboro, VT, USA) and focused to the cell culture dish. In both cases, the energy was adjusted to deliver 5%–10% uncaging of the caged-IP_3 amount loaded into the cells. All experiments were performed on HeLa-Cx43 cells, as HEK-Cx43 cells were found to be more sensitive to UV exposure. Control experiments loaded with vehicle-only showed that UV illumination by itself did not trigger any ATP-release in HeLa-Cx43 cells.

4.10 | ATP measurements

Hemichannel ATP-release was measured using a bioluminescent ATP assay kit (Sigma-Aldrich, Bornem, Belgium, Cat no. FLAAM) in the medium above the cells as previously described.[58] ATP-release was measured directly in the medium above the cells. Briefly, 75 µL ATP assay mix prepared in HBSS-HEPES (at fivefold dilution) was added to 150 µL medium above the cells and photon flux was counted (Victor-3, type 1420 multilabel counter, Perkin-Elmer, Brussels, Belgium).

4.11 | Whole-cell voltage clamp experiments

Cells were studied under whole-cell voltage-clamp to record membrane currents. HeLa-Cx43 cells were bathed in a recording chamber filled with a modified Krebs–Ringer solution consisting of (in mM): 150 NaCl, 4 CsCl, 2 $CaCl_2$, 2 $MgCl_2$, 2 pyruvate, 5 glucose and 5 HEPES; pH adjusted to 7.4. The standard whole-cell recording pipette solution was composed of (in mM): 130 CsCl, 10 Na-aspartate, 0.26 $CaCl_2$, 1 $MgCl_2$, 2 EGTA, 5 tetraethylammonium (TEA)-Cl and 5 HEPES; pH was adjusted to 7.2. For the experiments with caged IP_3 and IP3RPEP6, the pipette solution was composed of (in mM): 120 CsCl, 10 Na-aspartate, 1 $MgCl_2$, 0.2 EGTA, 10 tetraethylammonium (TEA)-Cl and 5 HEPES; pH was adjusted to 7.2. Caged IP_3 and IP3RPEP6 were applied by their inclusion in the whole-cell recording pipette solution.

Single channel recordings were performed with an EPC 7 PLUS patch-clamp amplifier (HEKA Elektronik, Lambrecht/Pfalz, Germany). Data were acquired at 4 kHz using a NI USB-6221 data acquisition device from National Instruments (Austin, TX, USA) and WinWCP or WinFluor software (credited to Dr. J. Dempster, Strathclyde Institute). All currents in whole-cell configuration were filtered at 1 kHz (7-pole Bessel filter). Patch pipette resistance was 2–5 MΩ; membrane potentials were corrected for liquid junction potentials.

For single channel analysis, holding currents were subtracted from the recorded current traces, giving traces that only contained unitary current events. Unitary conductances were calculated from the elementary current transitions Δi as: $\gamma = \Delta i / V_m$. From these data, we constructed all-point conductance histograms that were fitted by a Gaussian probability density function assuming independent channel opening. Channel activity was quantified from the charge transfer Q_m associated with unitary currents; this was done by integrating the unitary current traces over the duration of the voltage step as: $Q_m = \int i dt$.

4.12 | Western blot analysis and antibodies

Whole cell lysates were prepared by treating confluent cell culture with RIPA buffer consisting of 25 mM Tris, 50 mM NaCl, 0.5% NP-40, 0.5% deoxycholate, 0.1% SDS, 5.5% β-glycerophosphate, 1 mM dithiothreitol, 10 µL mL^{-1} protease inhibitor cocktail (Sigma-Aldrich), 30 µL mL^{-1} phosphatase inhibitor cocktail (Sigma-Aldrich) and 20 µL mL^{-1} mini EDTA-free protease inhibitor cocktail. Cell lysates were analyzed by western blotting as previously described.[79] Briefly, proteins (10–20 µg) were separated by NuPAGE 4%–12% Bis/Tris SDS-polyacrylamide gels using MES/SDS-running buffer (Invitrogen) and transferred onto a polyvinylidene fluoride (PVDF) membrane. After blocking with TBS containing 0.1% Tween and 5% non-fat dry milk powder, the membrane was incubated with the primary antibody overnight. Next, membranes were incubated for 1 h with secondary horseradish peroxidase (HRP)-conjugated antibody (dilution 1:2000 in 0.1% Tween/TBS). Protein detection was performed with Pierce ECL Western Blotting Substrate (Thermo Fisher Scientific; p/a Perbio Science BVBA, Erembodegem, Belgium). Band quantification was done with ImageJ software.

Primary antibodies used in this study were: rabbit polyclonal anti-Cx43 (1:5000; Sigma-Aldrich Cat# C6219, RRID:AB_476857); rabbit polyclonal anti-Cx37 (1:500; Invitrogen Cat# 40-4300, RRID:AB_2533465); rabbit anti-Cx45 (1:100; Abcam Cat# ab70365); rabbit polyclonal anti-Cx40 (1:1000; Bioss Antibodies Cat# BS-1050R, RRID:AB_10857532); rabbit anti-IP_3R1 generated by Dr. Jan Parys's laboratory (1:1000; Rbt03)[80,81]; rabbit polyclonal anti-IP_3R2 (1:1000; Abiocode Cat# R2872-2, RRID:AB_2935642); mouse monoclonal anti-IP_3R3 (1:1000; BD Biosciences Cat# 610313, RRID:AB_397705); mouse monoclonal anti-GAPDH (1:10000; Abcam Cat# ab8245, RRID:AB_2107448); mouse monoclonal anti-vinculin (1:1000; Sigma-Aldrich Cat# V9131, RRID:AB_477629).

17481716, 0, Downloaded from https://onlinelibrary.wiley.com/doi/10.1111/apha.14086 by Ku Leuven, Wiley Online Library on [02/02/2024]. See the Terms and Conditions (https://onlinelibrary.wiley.com/terms-and-conditions) on Wiley Online Library for rules of use; OA articles are governed by the applicable Creative Commons License

4.13 | Biotin-pull-down assays

Two million cells of HEK-IP_3R2, HEK-Cx43 or astrocytes were plated in 75 cm^2 bottles. Cells were harvested and lysed in RIPA buffer after being confluent. Biotinylated peptides (further referred to as Biotin-IP3RPEP6 and the inactive version as Biotin-IP3RPEP6-E4K), used as bait, were immobilized on neutravidin agarose beads (Thermo Fisher Scientific, Pierce, Erembodegem, Belgium) (30 µL) for 1 h at 4°C. Immobilized peptides and cell lysates were used to perform biotin-pull-down assays as previously described.[82] Briefly, equimolar amounts of Biotin-IP3RPEP6 and Biotin-IP3RPEP6-E4K were incubated at 4°C with 500 µg cell lysates in 400 µL interaction buffer 0.025% NP-40 overnight. The beads were then washed five times with interaction buffer. The peptide-protein complexes were eluted in 30 µL LDS (Invitrogen/Thermo Fisher Scientific, Merelbeke, Belgium) supplemented with 1:200 β-mercaptoethanol by boiling for 5 min at 95°C. Samples were analyzed via western blotting using rabbit anti-IP_3R1 generated by Dr. Jan Parys's laboratory (1:1000; Rbt03)[80,81]; rabbit polyclonal anti-IP_3R2 (1:1000; Abiocode Cat# R2872-2, RRID:AB_2935642); mouse monoclonal anti-IP_3R3 (1:1000; BD Biosciences Cat# 610313, RRID:AB_397705). Quantifications were performed using the ImageJ software.

4.14 | Quantification and statistical analysis

Data are expressed as mean ± SEM. The sample size "*N*," that is, the number of experimental units, corresponds to the number of independent cell culture dishes used for the experiments.[83] The meaning of "*n*" depends on the type of experiment: for Ca^{2+} imaging experiments, it corresponds to the number of different cells recorded from on the day of the experiment for each condition. For ATP-release experiments, it corresponds to the number of replicate wells used on the experimental day. For patch-clamp electrophysiology, it denotes the cells recorded from per experimental day for each condition. For every experimental day, we calculated the average over "*n*" experiments performed on that particular day.[83] Statistical analysis was performed based on the data from all experimental days reported by "*N*."

Statistical analysis was done with Prism software (GraphPad 5.0). Two groups were compared with an unpaired Student's *t*-test and two-tailed *p*-value depending on the experiment design. Multiple groups were compared by one-way analysis of variance (ANOVA) with post-hoc Dunnett's multiple comparison test. For analysis of concentration-effect relationships, non-linear curve-fitting to a Hill equation was used to provide values for EC_{50} (half-maximal effective concentration) or IC_{50} (half-maximal inhibitory concentration). Results were considered statistically significant at $p < 0.05$ (*), $p < 0.01$ (†), $p < 0.001$ (‡) and $p < 0.0001$ (****), or not significant at $p > 0.05$ (ns).

AUTHOR CONTRIBUTIONS

Conceptualization, L.L., P.H. and S.T.; Methodology, S.T., G.B., L.E.W. and D.I.Y.; Investigation, S.T., P.H. and L.E.W.; Writing—Original Draft, L.L. and S.T.; Writing—Review and Editing, K.W., G.B. and L.L.; Funding Acquisition, K.W., G.B. and L.L.; Supervision, K.W., G.B. and L.L.

ACKNOWLEDGMENTS

We thank Ellen Cocquyt and Diego De Baere (Ghent University) for their superb technical support and Rita La Rovere and Tomas Luyten (KULeuven) for their excellent expertise and support related to the pull-down assays and ER calcium measurements respectively. We acknowledge Dr. S.R. Wayne Chen, University of Calgary, Canada for donation of the inducible RyR2 expressing HEK cells.

Research supported by Research Foundation—Flanders (FWO) to L.L. (grant numbers G052718N, G040720N, G063023N) and G.B. (G090118N, G0E7520N, G081821N, G094522N). K.W. is supported by a Ghent University postdoctoral fellowship. Research in the G.B. lab was further supported by the KU Leuven Research Council (C14/19/099 and AKUL/19/34) and the Central European Leuven Strategic Alliance (CELSA/23/031). L.L., G.B. and D.I.Y. are partners of the FWO Scientific Research Network CaSign (W0.019.17N and W0.014.22N). S.T. acknowledges financial support from China Scholarship Council (CSC no. 201906170050).

CONFLICT OF INTEREST STATEMENT

A patent application no. EP23169580 is pending for intellectual property protection of the IP3RPEP6 peptide presented in this study, involving the following authors of this study: Siyu TAO, Paco HULPIAU, Katja WITSCHAS, Geert BULTYNCK and Luc LEYBAERT.

DATA AVAILABILITY STATEMENT

All data supporting the findings of this study are available from the corresponding author upon reasonable request.

ORCID

Paco Hulpiau https://orcid.org/0000-0002-6692-2150
Katja Witschas https://orcid.org/0000-0002-0960-683X
Luc Leybaert https://orcid.org/0000-0001-6452-6982

17481716, 0, Downloaded from https://onlinelibrary.wiley.com/doi/10.1111/apha.14086 by Ku Leuven, Wiley Online Library on [02/02/2024]. See the Terms and Conditions (https://onlinelibrary.wiley.com/terms-and-conditions) on Wiley Online Library for rules of use; OA articles are governed by the applicable Creative Commons License

REFERENCES

1. Foskett JK, White C, Cheung KH, Mak DOD. Inositol trisphosphate receptor Ca^{2+} release channels. *Physiol Rev*. 2007;87(2):593-658.
2. Hamada K, Mikoshiba K. IP(3) receptor plasticity underlying diverse functions. *Annu Rev Physiol*. 2020;82:151-176.
3. Berridge MJ. The inositol trisphosphate/calcium signaling pathway in health and disease. *Physiol Rev*. 2016;96(4):1261-1296.
4. Garcia MI, Boehning D. Cardiac inositol 1,4,5-trisphosphate receptors. *Biochim Biophys Acta Mol Cell Res*. 2017;1864(6):907-914.
5. Parys JB, De Smedt H. Inositol 1,4,5-trisphosphate and its receptors. *Adv Exp Med Biol*. 2012;740:255-279.
6. Gambardella J, Lombardi A, Morelli MB, Ferrara J, Santulli G. Inositol 1,4,5-trisphosphate receptors in human disease: a comprehensive update. *J Clin Med*. 2020;9(4):1096.
7. Ivanova H, Vervliet T, Missiaen L, Parys JB, De Smedt H, Bultynck G. Inositol 1,4,5-trisphosphate receptor-isoform diversity in cell death and survival. *Biochim Biophys Acta*. 2014;1843(10):2164-2183.
8. Bartok A, Weaver D, Golenár T, et al. IP(3) receptor isoforms differently regulate ER-mitochondrial contacts and local calcium transfer. *Nat Commun*. 2019;10(1):3726.
9. Serysheva II, Baker MR, Fan G. Structural insights into IP(3)R function. *Adv Exp Med Biol*. 2017;981:121-147.
10. Fan G, Baker ML, Wang Z, et al. Gating machinery of InsP3R channels revealed by electron cryomicroscopy. *Nature*. 2015;527(7578):336-341.
11. Hamada K, Miyatake H, Terauchi A, Mikoshiba K. IP(3)-mediated gating mechanism of the IP(3) receptor revealed by mutagenesis and X-ray crystallography. *Proc Natl Acad Sci U S A*. 2017;114(18):4661-4666.
12. Kang M, Lin N, Li C, et al. Cx43 phosphorylation on S279/282 and intercellular communication are regulated by IP3/IP3 receptor signaling. *Cell Commun Signal*. 2014;12:58.
13. Michelangeli F, Mezna M, Tovey S, Sayers LG. Pharmacological modulators of the inositol 1,4,5-trisphosphate receptor. *Neuropharmacology*. 1995;34(9):1111-1122.
14. Ghosh TK, Eis PS, Mullaney JM, Ebert CL, Gill DL. Competitive, reversible, and potent antagonism of inositol 1,4,5-trisphosphate-activated calcium release by heparin. *J Biol Chem*. 1988;263(23):11075-11079.
15. Maruyama T, Kanaji T, Nakade S, Kanno T, Mikoshiba K. 2APB, 2-aminoethoxydiphenyl borate, a membrane-penetrable modulator of ins(1,4,5)P3-induced Ca^{2+} release. *J Biochem*. 1997;122(3):498-505.
16. Parker I, Ivorra I. Caffeine inhibits inositol trisphosphate-mediated liberation of intracellular calcium in Xenopus oocytes. *J Physiol*. 1991;433:229-240.
17. Gafni J, Munsch JA, Lam TH, et al. Xestospongins: potent membrane permeable blockers of the inositol 1,4,5-trisphosphate receptor. *Neuron*. 1997;19(3):723-733.
18. Gambardella J, Morelli MB, Wang X, Castellanos V, Mone P, Santulli G. The discovery and development of IP3 receptor modulators: an update. *Expert Opin Drug Discov*. 2021;16(6):709-718.
19. Bultynck G, Sienaert I, Parys JB, et al. Pharmacology of inositol trisphosphate receptors. *Pflugers Arch*. 2003;445(6):629-642.
20. Ivanova H, Wagner LE 2nd, Tanimura A, et al. Bcl-2 and IP(3) compete for the ligand-binding domain of IP(3) Rs modulating Ca(2+) signaling output. *Cell Mol Life Sci*. 2019;76(19):3843-3859.
21. Azumaya CM, Linton EA, Risener CJ, Nakagawa T, Karakas E. Cryo-EM structure of human type-3 inositol triphosphate receptor reveals the presence of a self-binding peptide that acts as an antagonist. *J Biol Chem*. 2020;295(6):1743-1753.
22. Leybaert L, Sanderson MJ. Intercellular Ca(2+) waves: mechanisms and function. *Physiol Rev*. 2012;92(3):1359-1392.
23. Bezprozvanny I, Watras J, Ehrlich BE. Bell-shaped calcium-response curves of ins(1,4,5)P3- and calcium-gated channels from endoplasmic reticulum of cerebellum. *Nature*. 1991;351(6329):751-754.
24. Keizer J, De Young GW. Two roles of Ca^{2+} in agonist stimulated Ca^{2+} oscillations. *Biophys J*. 1992;61(3):649-660.
25. Goldbeter A, Dupont G, Berridge MJ. Minimal model for signal-induced Ca^{2+} oscillations and for their frequency encoding through protein phosphorylation. *Proc Natl Acad Sci U S A*. 1990;87(4):1461-1465.
26. De Bock M, Wang N, Bol M, et al. Connexin 43 hemichannels contribute to cytoplasmic Ca^{2+} oscillations by providing a bimodal Ca^{2+}–dependent Ca^{2+} entry pathway. *J Biol Chem*. 2012;287(15):12250-12266.
27. Bol M, Wang N, De Bock M, et al. At the cross-point of connexins, calcium, and ATP: blocking hemichannels inhibits vasoconstriction of rat small mesenteric arteries. *Cardiovasc Res*. 2017;113(2):195-206.
28. De Bock M, Culot M, Wang N, et al. Connexin channels provide a target to manipulate brain endothelial calcium dynamics and blood-brain barrier permeability. *J Cereb Blood Flow Metab*. 2011;31(9):1942-1957.
29. Turovsky EA, Varlamova EG, Turovskaya MV. Activation of Cx43 hemichannels induces the generation of Ca(2+) oscillations in white adipocytes and stimulates lipolysis. *Int J Mol Sci*. 2021;22(15):8095.
30. De Bock M, Wang N, Decrock E, et al. Endothelial calcium dynamics, connexin channels and blood-brain barrier function. *Prog Neurobiol*. 2013;108:1-20.
31. Braet K, Vandamme W, Martin PEM, Evans WH, Leybaert L. Photoliberating inositol-1,4,5-trisphosphate triggers ATP release that is blocked by the connexin mimetic peptide gap 26. *Cell Calcium*. 2003;33(1):37-48.
32. De Smet MA, Lissoni A, Nezlobinsky T, et al. Cx43 hemichannel microdomain signaling at the intercalated disc enhances cardiac excitability. *J Clin Invest*. 2021;131(7):e137752.
33. Srinivas M, Calderon DP, Kronengold J, Verselis VK. Regulation of connexin hemichannels by monovalent cations. *J Gen Physiol*. 2006;127(1):67-75.
34. Li F, Sugishita K, Su Z, Ueda I, Barry WH. Activation of connexin-43 hemichannels can elevate [Ca(2+)]i and [Na(+)]i in rabbit ventricular myocytes during metabolic inhibition. *J Mol Cell Cardiol*. 2001;33(12):2145-2155.
35. John SA, Kondo R, Wang SY, Goldhaber JI, Weiss JN. Connexin-43 hemichannels opened by metabolic inhibition. *J Biol Chem*. 1999;274(1):236-240.
36. Kondo RP, Wang SY, John SA, Weiss JN, Goldhaber JI. Metabolic inhibition activates a non-selective current through connexin hemichannels in isolated ventricular myocytes. *J Mol Cell Cardiol*. 2000;32(10):1859-1872.
37. Eltzschig HK, Eckle T, Mager A, et al. ATP release from activated neutrophils occurs via connexin 43 and modulates

17481716, 0, Downloaded from https://onlinelibrary.wiley.com/doi/10.1111/apha.14086 by Ku Leuven, Wiley Online Library on [02/02/2024]. See the Terms and Conditions (https://onlinelibrary.wiley.com/terms-and-conditions) on Wiley Online Library for rules of use; OA articles are governed by the applicable Creative Commons License

adenosine-dependent endothelial cell function. *Circ Res*. 2006;99(10):1100-1108.
38. Kang J, Kang N, Lovatt D, et al. Connexin 43 hemichannels are permeable to ATP. *J Neurosci*. 2008;28(18):4702-4711.
39. Gossman DG, Zhao H-B. Hemichannel-mediated inositol 1,4,5-trisphosphate (IP3) release in the cochlea: a novel mechanism of IP3 intercellular signaling. *Cell Commun Adhes*. 2008;15(4):305-315.
40. Saladin A, Rey J, Thévenet P, Zacharias M, Moroy G, Tufféry P. PEP-SiteFinder: a tool for the blind identification of peptide binding sites on protein surfaces. *Nucleic Acids Res*. 2014;42:W221-W226.
41. Lamiable A, Thévenet P, Eustache S, Saladin A, Moroy G, Tuffery P. Peptide suboptimal conformation sampling for the prediction of protein-peptide interactions. *Methods Mol Biol*. 2017;1561:21-34.
42. Webb B, Sali A. Comparative protein structure modeling using MODELLER. *Curr Protoc Bioinformatics*. 2016;54:5.6.1-5.6.37.
43. Wagner LE 2nd, Yule DI. Differential regulation of the $InsP_3$ receptor type-1 and -2 single channel properties by $InsP_3$, Ca^{2+} and ATP. *J Physiol*. 2012;590(14):3245-3259.
44. Alzayady KJ, Wagner LE 2nd, Chandrasekhar R, et al. Functional inositol 1,4,5-trisphosphate receptors assembled from concatenated homo- and heteromeric subunits. *J Biol Chem*. 2013;288(41):29772-29784.
45. Atakpa P, Thillaiappan NB, Mataragka S, Prole DL, Taylor CW. IP(3) receptors preferentially associate with ER-lysosome contact sites and selectively deliver Ca(2+) to lysosomes. *Cell Rep*. 2018;25(11):3180-3193.e7.
46. Alzayady KJ, Wang L, Chandrasekhar R, Wagner LE 2nd, Van Petegem F, Yule DI. Defining the stoichiometry of inositol 1,4,5-trisphosphate binding required to initiate Ca^{2+} release. *Sci Signal*. 2016;9(422):ra35.
47. Decrock E, De Bock M, Wang N, Bol M, Gadicherla AK, Leybaert L. Electroporation loading and flash photolysis to investigate intra- and intercellular Ca^{2+} signaling. *Cold Spring Harb Protoc*. 2015;2015(3):239-249.
48. Decrock E, De Vuyst E, Vinken M, et al. Connexin 43 hemichannels contribute to the propagation of apoptotic cell death in a rat C6 glioma cell model. *Cell Death Differ*. 2009;16(1):151-163.
49. De Vuyst E, De Bock M, Decrock E, et al. In situ bipolar electroporation for localized cell loading with reporter dyes and investigating gap junctional coupling. *Biophys J*. 2008;94(2):469-479.
50. Jiang D, Xiao B, Yang D, et al. RyR2 mutations linked to ventricular tachycardia and sudden death reduce the threshold for store-overload-induced Ca^{2+} release (SOICR). *Proc Natl Acad Sci U S A*. 2004;101(35):13062-13067.
51. Leybaert L, De Smet MA, Lissoni A, et al. Connexin hemichannels as candidate targets for cardioprotective and antiarrhythmic treatments. *J Clin Invest*. 2023;133(6):e168117.
52. Wang N, De Vuyst E, Ponsaerts R, et al. Selective inhibition of Cx43 hemichannels by Gap19 and its impact on myocardial ischemia/reperfusion injury. *Basic Res Cardiol*. 2013;108(1):309.
53. Catarino S, Ramalho JS, Marques C, Pereira P, Girão H. Ubiquitin-mediated internalization of connexin43 is independent of the canonical endocytic tyrosine-sorting signal. *Biochem J*. 2011;437(2):255-267.
54. Wallraff A, Köhling R, Heinemann U, Theis M, Willecke K, Steinhäuser C. The impact of astrocytic gap junctional coupling on potassium buffering in the hippocampus. *J Neurosci*. 2006;26(20):5438-5447.
55. Sherwood MW, Arizono M, Panatier A, Mikoshiba K, Oliet SHR. Astrocytic IP(3)Rs: beyond IP(3)R2. *Front Cell Neurosci*. 2021;15:695817.
56. Sherwood MW, Arizono M, Hisatsune C, et al. Astrocytic IP(3)Rs: contribution to Ca(2+) signalling and hippocampal LTP. *Glia*. 2017;65(3):502-513.
57. Takano T, Wallace JT, Baldwin KT, et al. Chemico-genetic discovery of astrocytic control of inhibition in vivo. *Nature*. 2020;588(7837):296-302.
58. De Vuyst E, Decrock E, Cabooter L, et al. Intracellular calcium changes trigger connexin 32 hemichannel opening. *EMBO J*. 2006;25(1):34-44.
59. De Vuyst E, Wang N, Decrock E, et al. Ca(2+) regulation of connexin 43 hemichannels in C6 glioma and glial cells. *Cell Calcium*. 2009;46(3):176-187.
60. Li H, Liu TF, Lazrak A, et al. Properties and regulation of gap junctional hemichannels in the plasma membranes of cultured cells. *J Cell Biol*. 1996;134(4):1019-1030.
61. Contreras JE, Sáez JC, Bukauskas FF, Bennett MVL. Gating and regulation of connexin 43 (Cx43) hemichannels. *Proc Natl Acad Sci U S A*. 2003;100(20):11388-11393.
62. Thimm J, Mechler A, Lin H, Rhee S, Lal R. Calcium-dependent open/closed conformations and interfacial energy maps of reconstituted hemichannels. *J Biol Chem*. 2005;280(11):10646-10654.
63. Saleem H, Tovey SC, Molinski TF, Taylor CW. Interactions of antagonists with subtypes of inositol 1,4,5-trisphosphate (IP3) receptor. *Br J Pharmacol*. 2014;171(13):3298-3312.
64. Bai D, del Corsso C, Srinivas M, Spray DC. Block of specific gap junction channel subtypes by 2-aminoethoxydiphenyl borate (2-APB). *J Pharmacol Exp Ther*. 2006;319(3):1452-1458.
65. Wang N, De Bock M, Decrock E, et al. Paracrine signaling through plasma membrane hemichannels. *Biochim Biophys Acta*. 2013;1828(1):35-50.
66. Abudara V, Bechberger J, Freitas-Andrade M, et al. The connexin43 mimetic peptide Gap19 inhibits hemichannels without altering gap junctional communication in astrocytes. *Front Cell Neurosci*. 2014;8:306.
67. Giaume C, Naus CC, Sáez JC, Leybaert L. Glial connexins and pannexins in the healthy and diseased brain. *Physiol Rev*. 2021;101(1):93-145.
68. Srinivasan R, Huang BS, Venugopal S, et al. Ca(2+) signaling in astrocytes from Ip3r2(−/−) mice in brain slices and during startle responses in vivo. *Nat Neurosci*. 2015;18(5):708-717.
69. Okubo Y, Kanemaru K, Suzuki J, Kobayashi K, Hirose K, Iino M. Inositol 1,4,5-trisphosphate receptor type 2-independent Ca(2+) release from the endoplasmic reticulum in astrocytes. *Glia*. 2019;67(1):113-124.
70. Okubo Y, Iino M. Visualization of astrocytic intracellular Ca(2+) mobilization. *J Physiol*. 2020;598(9):1671-1681.
71. Golovina VA, Blaustein MP. Spatially and functionally distinct Ca^{2+} stores in sarcoplasmic and endoplasmic reticulum. *Science*. 1997;275(5306):1643-1648.
72. De Bock M, De Smet M, Verwaerde S, et al. Targeting gliovascular connexins prevents inflammatory blood-brain barrier leakage and astrogliosis. *JCI Insight*. 2022;7(16):e135263.

17481716, 0, Downloaded from https://onlinelibrary.wiley.com/doi/10.1111/apha.14086 by Ku Leuven, Wiley Online Library on [02/02/2024]. See the Terms and Conditions (https://onlinelibrary.wiley.com/terms-and-conditions) on Wiley Online Library for rules of use; OA articles are governed by the applicable Creative Commons License

73. Betzenhauser MJ, Wagner LE 2nd, Iwai M, Michikawa T, Mikoshiba K, Yule DI. ATP modulation of Ca^{2+} release by type-2 and type-3 inositol (1, 4, 5)-triphosphate receptors. Differing ATP sensitivities and molecular determinants of action. *J Biol Chem*. 2008;283(31):21579-21587.
74. Chandrasekhar R, Alzayady KJ, Wagner LE 2nd, Yule DI. Unique regulatory properties of heterotetrameric inositol 1,4,5-trisphosphate receptors revealed by studying concatenated receptor constructs. *J Biol Chem*. 2016;291(10):4846-4860.
75. Le HT, Sin WC, Lozinsky S, et al. Gap junction intercellular communication mediated by connexin43 in astrocytes is essential for their resistance to oxidative stress. *J Biol Chem*. 2014;289(3):1345-1354.
76. Schildge S, Bohrer C, Beck K, Schachtrup C. Isolation and culture of mouse cortical astrocytes. *J Vis Exp*. 2013;71:50079.
77. Fan G, Baker MR, Wang Z, et al. Cryo-EM reveals ligand induced allostery underlying InsP(3)R channel gating. *Cell Res*. 2018;28(12):1158-1170.
78. Betzenhauser MJ, Wagner LE 2nd, Park HS, Yule DI. ATP regulation of type-1 inositol 1,4,5-trisphosphate receptor activity does not require walker A-type ATP-binding motifs. *J Biol Chem*. 2009;284(24):16156-16163.
79. Monaco G, Decrock E, Akl H, et al. Selective regulation of IP3-receptor-mediated Ca^{2+} signaling and apoptosis by the BH4 domain of Bcl-2 versus Bcl-xl. *Cell Death Differ*. 2012;19(2):295-309.
80. Sipma H, De Smet P, Sienaert I, et al. Modulation of inositol 1,4,5-trisphosphate binding to the recombinant ligand-binding site of the type-1 inositol 1,4,5-trisphosphate receptor by Ca^{2+} and calmodulin. *J Biol Chem*. 1999;274(17):12157-12162.
81. Parys JB, de Smedt H, Missiaen L, Bootman MD, Sienaert I, Casteels R. Rat basophilic leukemia cells as model system for inositol 1,4,5-trisphosphate receptor IV, a receptor of the type II family: functional comparison and immunological detection. *Cell Calcium*. 1995;17(4):239-249.
82. Ivanova H, Ritaine A, Wagner L, et al. The trans-membrane domain of Bcl-2α, but not its hydrophobic cleft, is a critical determinant for efficient IP3 receptor inhibition. *Oncotarget*. 2016;7(34):55704-55720.
83. Lazic SE, Clarke-Williams CJ, Munafò MR. What exactly is 'N' in cell culture and animal experiments? *PLoS Biol*. 2018;16(4):e2005282.
84. Zissimopoulos S, Seifan S, Maxwell C, Williams AJ, Lai FA. Disparities in the association of the ryanodine receptor and the FK506-binding proteins in mammalian heart. *J Cell Sci*. 2012;125(Pt 7):1759-1769.
85. Li J, Imtiaz MS, Beard NA, et al. ß-adrenergic stimulation increases RyR2 activity via intracellular Ca^{2+} and Mg^{2+} regulation. *PLoS ONE*. 2013;8(3):e58334.

SUPPORTING INFORMATION

Additional supporting information can be found online in the Supporting Information section at the end of this article.

How to cite this article: Tao S, Hulpiau P, Wagner LE II, et al. IP3RPEP6, a novel peptide inhibitor of IP_3 receptor channels that does not affect connexin-43 hemichannels. *Acta Physiol*. 2024;00:e14086. doi:10.1111/apha.14086

17481716, 0, Downloaded from https://onlinelibrary.wiley.com/doi/10.1111/apha.14086 by Ku Leuven, Wiley Online Library on [02/02/2024]. See the Terms and Conditions (https://onlinelibrary.wiley.com/terms-and-conditions) on Wiley Online Library for rules of use; OA articles are governed by the applicable Creative Commons License